3.2 and 3.3 Combustion Inorganic Transformation

COMBUSTION INORGANIC TRANSFORMATIONS

Annual Technical Report for the Period
July 1, 1989 through June 30, 1990
Including
the Seventeenth Quarterly Technical Progress Report
for the Period April through June 1990

by

Chris J. Zygarlicke, Steven A. Benson, Donald L. Toman,
Edward N. Steadman, David W. Brekke, Thomas A. Erickson, and John P. Hurley

Combustion and Environmental Systems Research Institute
Energy and Environmental Research Center
University of North Dakota
Box 8213, University Station
Grand Forks, ND 58202

Contracting Officer's Representative: Philip M. Goldberg

for

U.S. Department of Energy
Office of Fossil Energy
Pennsylvania Energy Technology Center
P.O. Box 10940, Mail Stop 922-H
Pittsburgh, PA 15236-0940

October 1990

Work Performed Under Cooperative Agreement No. DE-FC21-86MC10637

TABLE OF CONTENTS

TABLE OF CONTENTS (Continued)

TABLE OF CONTENTS (Continued)

LIST OF FIGURES

LIST OF FIGURES (Continued)

LIST OF FIGURES (Continued)

LIST OF FIGURES (Continued)

LIST OF FIGURES (Continued)

LIST OF FIGURES (Continued)

LIST OF TABLES

LIST OF TABLES (Continued)

LIST OF TABLES (Continued)

LIST OF TABLES (Continued)

LIST OF TABLES (Continued)

COMBUSTION INORGANIC TRANSFORMATIONS

Submitted by: Steven A. Benson, Principal Investigator

Prepared by: Chris J. Zygarlicke, Edward N. Steadman, John P. Hurley, Thomas. A. Erickson, David A. Brekke, Donald L. Toman, Dennis Brostuen, and Bruce Folkadahl

EXECUTIVE SUMMARY

Task 1: Improvements to the CCSEM Methodology

The work that was proposed this year under Task 1 was:

1) Rigorous testing of the present CCSEM analysis, which includes the use of mineral standards and well-characterized coals.

2) Software and hardware development to allow for stage automation, multiple threshold capabilities, and data manipulation.

3) Eliminating size biases associated with irregularly shaped grains and sample preparation.

4) Modification of existing software to determine juxtaposition of mineral grains.

5) Developing software that will graphically represent the elemental composition of mineral and ash components.

All of the proposed goals listed above were accomplished in full except for #3, which was completed for the most part; however, questions remain as to the type of correction factor(s) needed for coal minerals. Work will continue into the next year to correctly evaluate size biases of coal minerals by CCSEM.

Mineral standards and coal samples were prepared and analyzed using a computer-controlled scanning electron microscopy (CCSEM) routine. The chemical typing criteria accurately classify the minerals tested. Some errors in the CCSEM routine appear to be related to the Tracor Northern PRC (Particle Recognition and Characterization) program and are probably the result of the magnifications and step sizes used. The repeatability tests showed poor accuracy in obtaining a mineral definition of the sample, but showed good repeatability in the bulk particle-size distributions obtained. New procedures and software are presently being developed to address these problems. Preliminary investigations into a round-robin testing of the present CCSEM method have been made.

Stage automation during the running of the CCSEM analysis was completed, which allows the analysis to be run unattended. Interfacing between CCSEM and image analysis is also completed. This allows the fields analyzed by the CCSEM routine to be stored in the image analysis system and data concerning the juxtaposition to be collected.

More graphic outputs for the CCSEM program have been developed, and work continues in this area. An improved version of the data manipulation program has been developed and thoroughly tested. Future programs will include some of the graphic methods as standard outputs.

Further development of coal minerals analysis may well focus on the sole use of the sophisticated imaging capabilities now available. Ultimately, the present chemical typing and sizing may be replaced by chemical typing and characterization on the new system. An intermediate step may be necessary which would combine the present analysis with modern imaging capabilities. The present chemical typing and characterization has the benefit of thousands of hours of use and testing. By combining it with the new imaging capabilities, we can solve one problem at a time and move forward in a logical, step-wise fashion. For these reasons, we will further explore the capabilities of the image analysis system while continuing to test and explore the capabilities of the present system.

Task 2: Mineral and Ash Characterization

Under Task 2 there were three major goals:

1) To perform CCSEM analysis on four coals provided by PSIT and coals used in Task 3 of this program. In addition, chemical fractionation will also be performed on lower-rank subbituminous and lignitic coals.

2) To perform CCSEM analysis of 40 ash samples provided by PSIT and ash samples generated at EERC in Task 3 of this project.

3) To perform additional analytical work on samples generated at PSIT and EERC using SEMPC, ESCA, SIMS, and AA/ICP. SEM morphology and elemental mapping will also be performed. In addition, low-temperature ashing of selected coals will be performed.

All of the above work goals were fulfilled except that submission of coal and ash samples by PSIT for CCSEM analysis fell far short of what was planned.

Fourteen deposits were analyzed for Physical Sciences Incorporated Technology Company (PSIT) for phase assemblage determination using scanning electron microscopy point count (SEMPC). The deposits were generated from the following coals: San Miguel, Beulah, Kentucky #11, Illinois #6, Kentucky #9, Eagle Butte, and Upper Freeport. Four fly ash samples were analyzed for PSIT using CCSEM. These samples were generated from the following coals: Kentucky #9, Eagle Butte, San Miguel, and Illinois #6.

Several coal chars and ashes generated in the EERC drop-tube furnace were analyzed by surface science techniques to determine particle surface chemistry and coating structure. The major techniques used during this reporting period were Auger electron spectroscopy (AES) and AES depth profiling utilizing an ion sputtergun. The char particles analyzed were typically 30-60 μm in diameter.

Small 0.1-2 μm ash particles observed on the surface of the Eagle Butte char were analyzed using AES. Calcium was a major constituent in the ash particles. Char particles nearing 90% carbon burnout show an enrichment of Ca at the outer 0.3-0.4 μm of their surface using AES depth profiling. Inhomogeneities, in the form of differential etching by the AES sputtergun, are consistently observed in the near surface zone of Eagle Butte fly ash particles. Beulah char shows the same Ca-rich coating as the Eagle Butte char. Chemical depth profiling of Beulah fly ash grains shows distinct variations in chemistry and physical resistance to the sputtering action of the Auger beam.

AES analysis of early-stage, small inorganic ash droplets in the Beulah and Robinson chars also shows very high Ca content.

Synthetic coal ash particles were analyzed with AES. The original material consisted of 10% SiO_2, 5% Na, and 1% S in a carbon matrix. Fly ash was produced in the drop-tube furnace using a combustion temperature of 1100°C and residence time of 1.5 seconds. Surface analysis revealed large particles of 30-40 μm in diameter coated with smaller particles less than 1 μm in size. The surface of the large particles was typically SiO_2 with some elemental Si present, possibly vaporized Si condensate, and virtually no carbon or sulfur. Small particles attached to larger fly ash grains were observed that were composed of SiO_2 and lesser amounts of sodium, sulfur, and carbon. The interior of the large grains revealed vesicular heterogeneous material of varying resistances to the argon ion sputtergun. The composition of the interior material was primarily SiO_2, with significant amounts of carbon and sodium.

Particle-size distributions of discrete mineral or amorphous phases in intermediates produced in the drop-tube furnace (DTF) for two coals were examined. Time-resolved PSD's of phases show that Beulah and Upper Freeport phases coalesce with time. The Upper Freeport shows an initial increase in the amount of particles in the lower size ranges due to fragmentation of minerals or the formation of smaller inorganic ash droplets from submicron minerals or inorganics. The transformation of selected inorganic components through time was also noted. Sodium and calcium organically associated in the Beulah react readily with smaller-sized kaolinitic clays and, to a much lesser degree, with quartz. Pyrite appears to undergo fragmentation during combustion in the Beulah and Upper Freeport, with a resulting increase in iron oxide.

Kentucky #9 and San Miguel coals were combusted at 1500°C and the fly ash particle size analyzed by CCSEM. The coal was sized with Malvern analysis, and the minerals in the coal were sized with CCSEM. The combustion of Kentucky #9 is highly dominated by the fragmentation process, with slight amounts of coalescence and possible fragmentation of a few of the larger mineral particles. The combustion of San Miguel lies between the two limiting regimes, demonstrating partial fragmentation followed by coalescence.

Task 3: Laboratory-Scale Combustion Testing

The proposed work plan for this past year under Task 3 included:

1) Characterization of two coals followed by combustion in the drop-tube furnace. Samples were to be extracted at residence times representative of devolatilization, partial burnout, and complete burnout. The fly ash was to be collected and sized using the multicyclone and impactor. The ash particles forming at the surface of the chars, as well as the "carbon-free" fly ash, were to be examined using the CCSEM/SEMPC techniques.

2) Determination of the factors influencing the formation of specific ash species.

   a. Sodium-rich ash phases: silicates, aluminosilicates, and sulfates.

   b. Iron-rich ash phases: silicates, aluminosilicates, and calcium aluminosilicates. Initial testing, including pyrite and quartz, will begin.

   c. Evaluate model predictions for simple oxide systems.

The combustion testing of the two coals, the Kentucky #9 and the San Miguel, was completed, as was the preparation and combustion testing of the synthetic char sodium-rich silicate-sulfate system. Combustion testing of calcium and iron-rich synthetic coal systems was reserved for this year.

Kentucky #9 coal contained about 15% ash and had high iron (20%) and moderate calcium (3%) and potassium (3%) contents on a normalized oxide basis. The most abundant minerals were quartz, aluminosilicate (degraded illite or mixed clay), illite, pyrite, and, for the 74-106 μm and unsized fraction, siderite. Ash content decreased with increasing coal size, but mineral sizes increased. Variability in mineral content was noted for the different coal sizes analyzed by CCSEM. An increase in pyrite with coal size corresponded with an increase in iron oxide in the coal ash.

Kentucky #9 fly ash showed interaction between iron in the pyrite with aluminosilicate to form Fe-aluminosilicates. Pyrite transformation was evidenced by reduction from 28% to 0%, and iron oxide was increased from 8% to 22% of the minerals. Kentucky #9 minerals that were <10 μm underwent coalescence to a size range mostly between 22-46 μm, while the largest Kentucky #9 minerals (>46 μm), which include pyrite and illite, underwent fragmentation. Time-resolved studies showed that K-aluminosilicate and iron oxide increased with time. Quartz content remained fairly constant from the coal to 0.8-second residence time char. The finest fraction of the Kentucky #9 size-segregated fly ash was enriched in CaO, SO_3, and TiO_2.

San Miguel lignite had about 53% ash on a dry basis and was very low in iron (1.9%) and calcium (3.5%). Sodium content was also low at 2.5% of the ash. Sodium and calcium were 65% and 72% organically bound, respectively.

The major minerals in the San Miguel lignite, as determined by CCSEM, were quartz, clinoptilolite, and an unknown aluminosilicate that was probably mixed clay or montmorillonite. Mineralogic compositions on a mineral basis were similar for 38-53, 53-74, and 74-106 μm coal fractions; however, larger minerals were observed with increased coal size. The total ash contents and elemental oxide chemistry were similar for the different coal size fractions.

Analysis of San Miguel short residence time char revealed that quartz and K-aluminosilicate contents remained fairly consistent through the combustion process, relative to their content in the original coal. Aluminosilicate was slightly reduced, and Fe-aluminosilicate and calcium silicate were slightly increased. The particle-size distributions of the inorganic phases in the chars showed coalescence with increased residence time. Smaller minerals between 1 and 10 μm decreased in abundance, and large inorganic phases between 22-46 μm increased in abundance progressively until 0.5 seconds into combustion. The 0.5 and 0.8 second chars were nearly identical in particle size and composition. This observation may be a result of near 100% carbon burnout by 0.5 seconds of combustion.

Fly ash was produced at a residence time of about 2.6 seconds at 1500°C gas temperature and collected on a bulk filter for the San Miguel 53-74 μm and unsized coals. In general, the fly ashes were similarly composed. Aluminosilicate and K-aluminosilicate decreased with combustion because of interaction with the other mineral components. SEMPC analysis of the size segregated fly ash from the multicyclone showed major phases of quartz or silica, amorphous illite, and amorphous montmorillonite. The amorphous illite was actually the derivative of potassium-rich zeolites in the coal. Most of the fly ash mass (89%) was greater than 22 μm in average diameter. It was observed that SiO_2 and K_2O oxides increased with increasing fly ash particle size, corresponding to greater amounts of the amorphous illite-derived phase. The finer fly ash fraction had more CaO and Al_2O_3.

Kentucky #9 and San Miguel coals were combusted at 1300, 1400 and 1500°C to produce fly ash which was collected in separate runs using a 5-stage multicyclone and an impactor. The Kentucky #9 multicyclone and cascade impactor data showed no change in particle-size distribution for different coal sizes or combustion temperatures. The San Miguel size distributions changed with both coal size and combustion temperature. The impactor and multicyclone data showed larger particle-size distributions for smaller initial coal size. Coalescence seems more prevalent for smaller coal sizes and lower temperatures, while fragmentation may dominate at higher temperatures and larger coal sizes.

Synthetic coal was produced by polymerizing furfuryl alcohol with p-toluenesulfonic acid, adding carbon black for porosity, and including quartz, sodium benzoate and sublimed sulfur as inorganic constituents. The synthetic coal was combusted at 900, 1100, 1300, and 1500°C for approximately 1.4 seconds, and chars at 0.1 and 0.5 seconds were also generated. The formation of sodium silicates during coal combustion was favored by longer residence times and higher temperatures. The formation of sodium sulfates did not interfere to any large degree with the formation of sodium silicates due to the high temperature of combustion taking place within the burning coal

environment. The formation of fly ash at the four temperatures appears to be governed by different mechanisms. At the lower temperatures, coalescence is dominating, while at the higher temperatures, fragmentation and shedding dominate. The formation of cenospheres at the lower temperatures may also affect the particle-size results. The exothermic reaction temperature of burning synthetic coal appears higher than that of coal, which may sway results towards the higher temperature regimes, but overall results of the synthetic coal appear good.

1.0 GOALS AND OBJECTIVES

The overall objective of this project is the development of a unified picture of the physical and chemical changes that occur in coal inorganic matter during combustion. The research focuses on three main tasks. The first task will involve developing the computer-controlled scanning electron methodology to determine the distribution of mineral grains in pulverized coals. The second task will involve determining the inorganic components in coal and coal ash-derived components for coals and ashes generated in the PETC mineral matter programs at EERC and Physical Sciences, Inc., Technology Company (PSIT). The third task will study the physical and chemical changes of inorganic phases during combustion in laboratory-scale combustion equipment.

The ultimate goal of the project is to develop a means to predict the state (vapor, liquid, or solid), composition, and size of the inorganic material at any point in a combustion system, given the coal composition and combustion conditions. The first task focuses on developing a method to effectively determine the size, composition, and juxtaposition of mineral grains in pulverized coals. In addition, chemical fractionation is used to determine the abundance of organically associated inorganic constituents in the lower-rank subbituminous and bituminous coals. Proper determination of the inorganic components in coal is an essential requirement in understanding and ultimately predicting the transformations of inorganic components during coal combustion. The second task involves characterizing coals, chars, and ashes. Coals will be examined by CCSEM and chemical fractionation to determine the association, size, composition, and juxtaposition of the inorganic components in coals.

Chars and ashes produced in Task 3 will be examined to determine their bulk composition, surface composition, phase distribution, and morphology. This will be accomplished primarily by utilizing surface science equipment, scanning electron microscopy/electron microprobe analysis, x-ray fluorescence, and x-ray diffraction. The objective of this task is to follow the transformation of inorganic constituents at various degrees of coal particle burnout to produce the fly ash. The third task involves using the drop-tube furnace system to produce chars at various degrees of burnout and ultimately a carbon-free fly ash. In addition, precisely formulated model mineral/coal mixtures are being produced and combusted to examine in detail some of the transformations that occur. In conjunction with these three tasks is an ongoing effort to evaluate all data produced, with respect to reproducibility, including coal characterization data, char and fly ash formation studies with the drop-tube furnace, and ash characterization data. A means of predicting the fate of

inorganic constituents during combustion cannot be adequately developed without consistent, quantitative data. During the past three years, this project has focused on developing consistent and quantitative techniques to produce and analyze the inorganic components in coals, chars, and fly ash. Data is currently available on seven coals, and one more will be examined this year. A modeling effort will be initiated this year to predict the size and composition of ash particles based on coal composition and combustion conditions. This effort will be coordinated with the work presently being conducted at EERC on viscosity modeling (1) and thermochemical equilibrium modeling (2).

1.1 Task 1: Improvements to the CCSEM Methodology

The specific objectives of the CCSEM improvements task during this year were to:

1) Evaluate the reproducibility of the CCSEM technique using coal samples.

2) Make arrangements for a limited round-robin testing of coal samples with other labs.

3) Complete interface of CCSEM computer with image analysis computer to allow for digital image collection.

1.2 Task 2: Mineral Ash Characterization

The specific objectives of the mineral and ash characterization task during this year were to:

1) Characterize deposit ash for PSIT using SEMPC.

2) Characterize surface materials of char and fly ash using AES, XPS, and SEM techniques.

3) Interpret results of coal characterization and combustion with a view to fly ash size and composition evolution.

1.3 Task 3: Laboratory-Scale Combustion Testing

The specific objectives of the laboratory-scale combustion testing task during this year were to:

1) Characterize the Kentucky #9 and San Miguel coals using chemical fractionation, CCSEM, and standard coal analysis techniques.

2) Produce intermediates for Kentucky #9 and San Miguel coal in the drop-tube furnace by combusting three size fractions at 1300, 1400, and 1500°C.

3) Produce intermediates for Kentucky #9 and San Miguel bulk coal samples in the drop-tube furnace and collect them on a bulk filter.

4) Produce short residence time chars for the Kentucky #9 and San Miguel coals in the drop-tube furnace at 1500°C for the 53-74 μm coal fraction.

5) Evaluate the particle size and composition evolution of fly ash using quartz, sulfur, and Na-enriched synthetic coal.

2.0 TASK 1: IMPROVEMENTS TO THE CCSEM METHODOLOGY

The objective of Task 1 is to provide precise characterization of the minerals present in pulverized coals and to coordinate an effort between laboratories performing CCSEM analysis on coal in order to develop a consistent methodology. Current methods of coal minerals characterization do not provide the level of detail needed to predict the interactions that take place during combustion. Mineral characteristics which affect their behavior during combustion include 1) chemical composition, 2) size, 3) association of minerals with coal matrix, 4) mineralogical associations, and 5) mineral shape. Presently, coal minerals are being characterized using a computer-controlled scanning electron microscope/microprobe method (CCSEM). CCSEM analysis gives mineral compositions and sizes. Task 1 seeks to enhance the present methodology to include other significant mineral characteristics such as the mineral associations, mineral shapes or morphology, and the relationship of the minerals to the coal matrix. Figure 1 outlines the proposed methodology for accomplishing Task 1. Please note the revisions of the completion data listed in Figure 1. The Task 1 project plan will use CCSEM together with an automated image acquisition and characterization program (AIA) to provide the data needed. Initial efforts are focused on testing the accuracy and precision of the present CCSEM methodology and on modifying the present method to include the capabilities of the image analysis system. This report will summarize accomplishments during the first year of the project.

2.1 Description Of System

2.1.1 JEOL/Tracor Northern System

The SEM/microprobe system at the EERC consists of a JEOL 35U scanning electron microscope/microprobe, a GW Electronics backscatter electron detector, an ultrathin window energy-dispersive x-ray detector, wavelength-dispersive x-ray detector, digital beam control, a Tracor-Northern 5600 x-ray microanalyzer control system, a Tracor-Northern 8500 image analyzer, and stage automation. The Tracor-Northern 5600 is interfaced with a MicroVax II and personal computer system for advanced data manipulation. Figure 2 outlines the SEM/microprobe system and its operations.

The key components of the SEM system that make it possible to image, size, and analyze inorganic particles include the backscatter electron detector, digital beam control, and the ultrathin window energy-dispersive x-ray detector. The Tracor-Northern 5600 allows for automated spectral acquisition and beam control, with data storage accomplished using the MicroVax II or PC. The Tracor-Northern 8500 image analysis system allows for the automated acquisition, storage, and processing of images from the SEM (Figure 2).

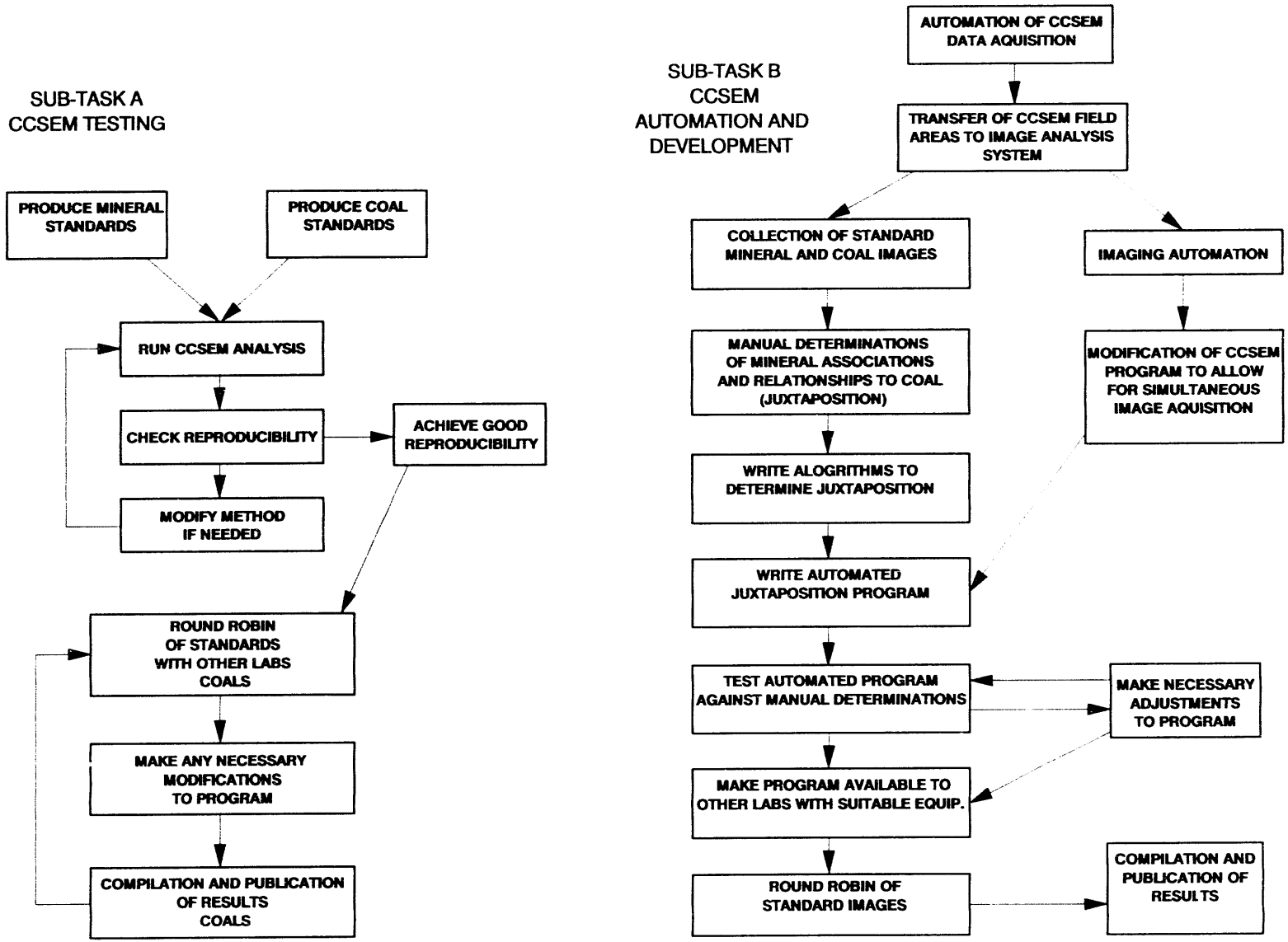

Figure 1. Task 1 - CCSEM methodology development.

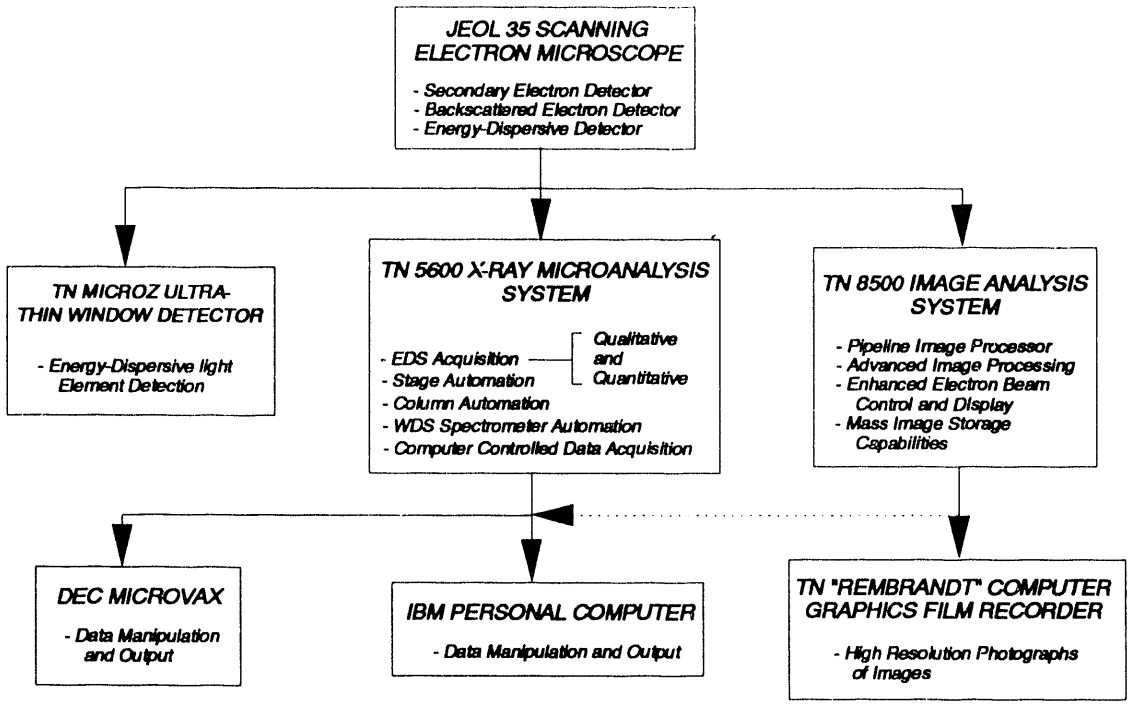

Figure 2. Schematic of SEM/microprobe system and its operation.

The CCSEM analysis uses backscattered electron imaging (BEI) and energy dispersive spectra (EDS) detection to analyze minerals. Since the mineral or ash particles appear brighter in BEI relative to the lower atomic number background of the matrix, a distinction can be made between coal, epoxy, and mineral grains. Using the Tracor-Northern particle recognition and characterization program, the electron beam is programmed to scan over the field of view to locate the bright inclusions that correspond to mineral or ash species. On finding a bright inclusion, the beam performs eight diameter measurements on the inclusion, finds the center of the inclusion, and collects an EDS for 2 seconds. The system is set up to analyze 12 elements: Na, Mg, Al, Si, P, S, Cl, K, Ca, Fe, Ba, and Ti. The associated computer system then outputs to a storage file the following information for each particle analyzed: size, area, perimeter, chemical composition, coordinates of location on the sample surface, frame number, and number of energy-photon counts.

Data from the CCSEM analysis is transferred simultaneously to a personal computer or the MicroVax II where it is stored on tape or disk. Software developed at EERC classifies the minerals into categories based on size and composition.

2.1.1.1 ADEM Description

In order to facilitate the development of fully automated SEM analysis routines using image analysis, an automated digital electron microscope (ADEM) was purchased and is now in use. The Tracor Northern ADEM is the first SEM to

obtain total system automation and computer control of all system parameters. The ADEM completely integrates analytical energy dispersive spectroscopy (EDS) and digital image processing. This totally automated and integrated system is needed for the further developments planned in the CCSEM development program. The JEOL/Tracor Northern system is not capable of changing beam parameters such as magnification, focus, and operating voltages in an automated, computer-controlled fashion. The control and monitoring of these parameters is integral for the planned CCSEM developments outlined in the description of subtask B, CCSEM automation and development. The ADEM provides further capabilities to the CCSEM development program because it is capable of the automated analysis of multiple samples; this will greatly increase the efficiency of our entire system and the amount of beam time available for research and technique development. Figure 3 shows a schematic of the ADEM and some of the system's capabilities.

2.2 Subtask A: CCSEM Testing

Testing of the CCSEM technique was focused on three different studies. The first study looked at the chemical typing of the CCSEM routine on three common mineral types. The second study looked at CCSEM reproducibility. The third study looked at the reproducibility of the Tracor Northern PRC program which is somewhat dependent upon operator setup.

In the first study, the three common minerals chosen for the chemical typing testing were pyrite, kaolinite, and quartz. The quartz sample was a fine powder (about -240 mesh) when obtained. To reduce the size of the kaolinite and pyrite, approximately 5 grams of sample were placed in a tungsten carbide ball mill for 3-5 minutes. The powdered samples were then sieved using a mechanical one-stage shaker with a 200-mesh and 400-mesh screen. The size cut generated had particle sizes of 37-74 μm. Evidence of agglomeration was observed during sieving; therefore, the true particle size is believed to be smaller.

The mineral samples were analyzed by SEMPC and XRD to determine their purity on the micron level. The quartz was found to be 99.6 wt% pure by SEMPC. The absence of any crystalline contaminants was verified by XRD. The only slight impurity was the presence of potassium aluminosilicate at a very minor level (0.3%). The kaolinite was found by XRD to be very pure also, with less than 0.5% impurities of iron, calcium, and magnesium. The pyrite standard was found to be made up of ferrous sulfate, pyrrhotite, pyrite, and iron oxide with small traces of silica and alumina (<0.2%). With CCSEM analysis (the chosen mineral standard technique), the pyrite was found to contain approximately 6% pyrrhotite and 1% iron oxide. For the purpose of analysis, all three of these iron-containing minerals will be considered pyrite.

A sample containing 33.3% by weight of quartz, kaolinite, and pyrite was made into an epoxy plug. Epo Thin (Beulher) was used as the epoxy because of its ability to allow air bubbles to escape the resin before hardening occurs. The sample (0.5 g total) was added to approximately 25 grams of Epo Thin in a glass vial, stirred slowly so as not to create bubbles, and rotated at 80 rpms on its axis so that gravitational settling was minimized. The sample was cut perpendicular to its axis and polished down to 0.25 microns with diamond

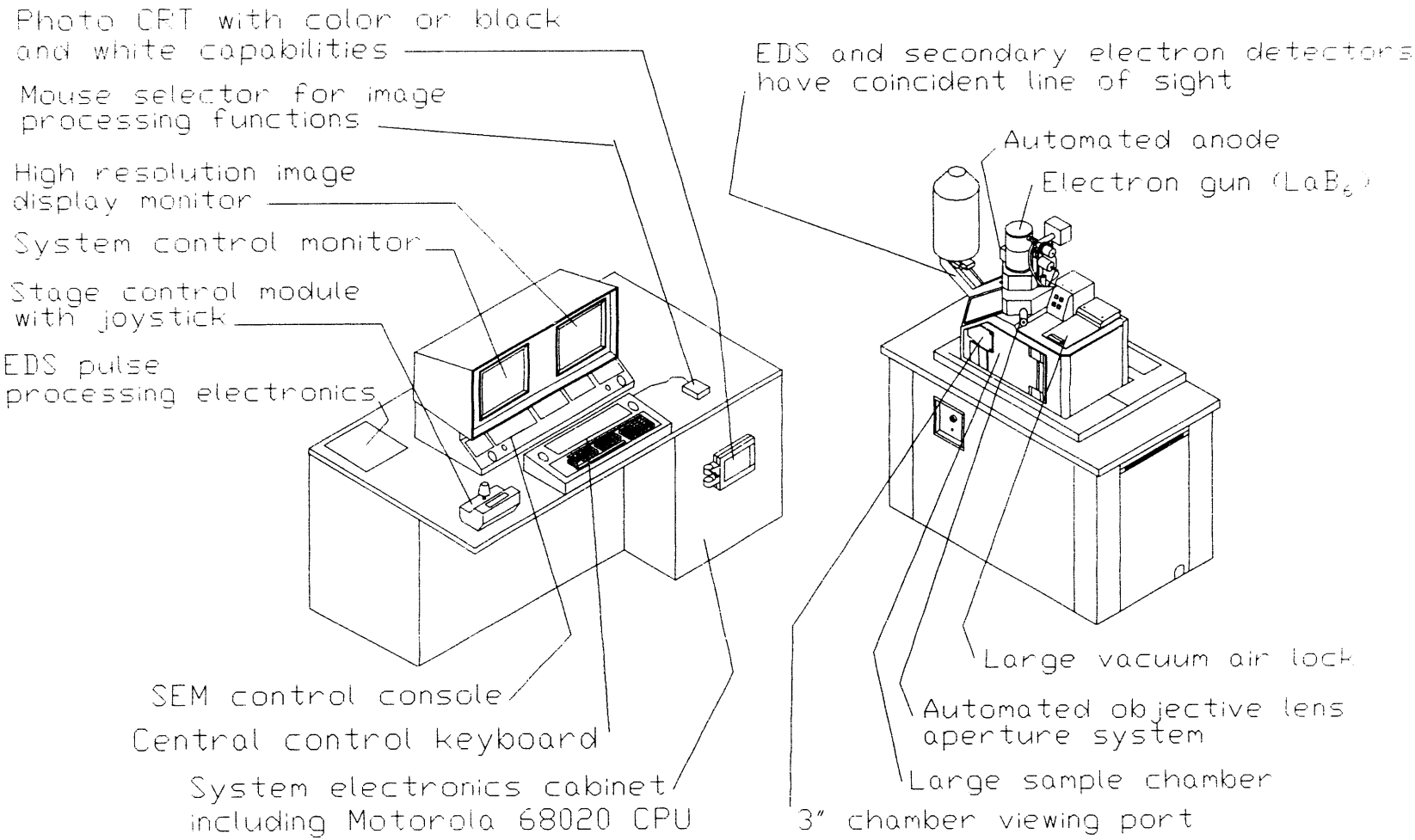

Figure 3. Schematic of the ADEM system.

polish. Due to the occasional release of mineral particles during polishing, some minor scratches were induced. The sample was coated with a thin layer of carbon with a diode-sputtering coater. Carbon was used because it does not interfere with the EDS spectral file collected.

The sample was analyzed with the CCSEM technique at 240x and 50x under 400 pA and 15 kV. The analysis found 29.5% quartz, 43.7% kaolinite, and 24.9% pyrite with less than 2% unidentified. These results indicate that the chemical typing works well, but the quantification is not very accurate for kaolinite and pyrite. The differences in percents of each mineral type found may be due to errors in the CCSEM analysis (PRC), sample preparation, shapes and cross-sectioning effects of the minerals, or a combination of all these factors. Future analysis of mineral standards will be designed to address these questions.

The particle sizes as determined by CCSEM were much smaller than the sizes determined by sieving which may indicate errors due to cross-sectioning effects. Ninety-five percent of the quartz was under 20 μm, while 75% and 85% of the kaolinite and pyrite, respectively, were under 20 μm. This was expected due to the agglomeration of minerals during sieving.

The second study focused on reproducibility of CCSEM data on a coal sample. CCSEM testing on mineral standards in previous Quarterly reports showed fairly good precision (3,4,5). Three coals have been selected to be tested. Splits of Beulah Lignite, Eagle Butte subbituminous, and Upper Freeport bituminous coals were prepared for CCSEM analysis. The later two are currently being tested. The Beulah was prepared in both epoxy and carnauba wax. The carnauba wax is used because it provides more contrast between coal and epoxy when viewing in the backscattered electron mode on the SEM.

Table 1 shows the results of the Beulah coal, prepared in an epoxy plug, tested on four different occasions. All four tests were done on separate days while all parameters of the analysis were kept constant. The average of the four tests is compared with the results obtained by PSI (6).

The results of the four individual tests show a large amount of scatter. The average analysis compares well with that of PSI with the exception of the pyrite, which may be explained by the large amount of unknowns high in both sulfur and iron content. With the average analysis matching closely with the PSI analysis, it would appear that the amount of area analyzed is the major factor. The amount of area needed to be analyzed is not known, but it would appear to have a lower limit of the area in any individual test and an upper limit of the area in the four tests.

Table 2 shows the particle-size distribution of the bulk minerals for the four test runs. This set of data is much closer than the chemical typing data as previously discussed. Figure 4 shows a graphical representation of the same data in the form of cumulative percent of minerals versus size. The sizes used in graphing are the mean diameter of the size bin. The error is highest in the smallest size bin as well as the large size bin at each magnification. Since two magnifications are used during the analysis, there are two separate sets of data. With the exception of the error in the

TABLE 1

CCSEM RESULTS OF BEULAH COAL
EPOXY MOUNTED

Major Phases	Test #1	Test #2	Test #3	Test #4	AVG	PSI
Quartz	8.3	2.0	19.9	16.3	11.6	12.8
Aluminosilicate	0.3	69.2	44.7	42.6	39.2	45.7
Ca-Aluminosilicate	1.4	2.3	5.4	0.5	2.4	1.1
K-Aluminosilicate	1.3	1.0	1.1	1.0	1.1	1.1
Pyrite + Periclase	28.2	11.5	10.6	24.2	18.6*	27.6
Ca-Rich	0.0	0.0	0.0	0.0	0.0	1.1
Unknowns & Minor Phases	30.5	14.0	18.3	15.4	19.6*	10.6
Mineral/Coal Basis	2.9	13.2	15.4	7.3	9.7	7.0

*Composition of Unknowns

Al	Si	S	Ca	Fe	Ba	Ti
6.4	25.7	20.8	6.7	16.0	7.5	7.32

TABLE 2

BEULAH LIGNITE PARTICLE-SIZE DISTRIBUTION

Size Bin (μm)	Test #1	Test #2	Test #3	Test #4	Average	Deviation	% Error
1 to 2.2	1.637	7.954	11.134	10.572	7.824	3.768	48.163
2.2 to 4.6	17.315	17.056	20.932	19.497	18.700	1.599	8.555
4.6 to 10.0	33.706	24.356	16.173	28.677	25.728	6.432	25.003
10.0 to 22.0	14.622	13.365	12.530	12.670	13.296	0.827	6.226
22.0 to 46.0	17.059	17.676	17.728	15.092	16.888	1.070	6.336
46.0 to 100.0	15.661	15.594	21.504	13.493	17.563	3.155	17.969

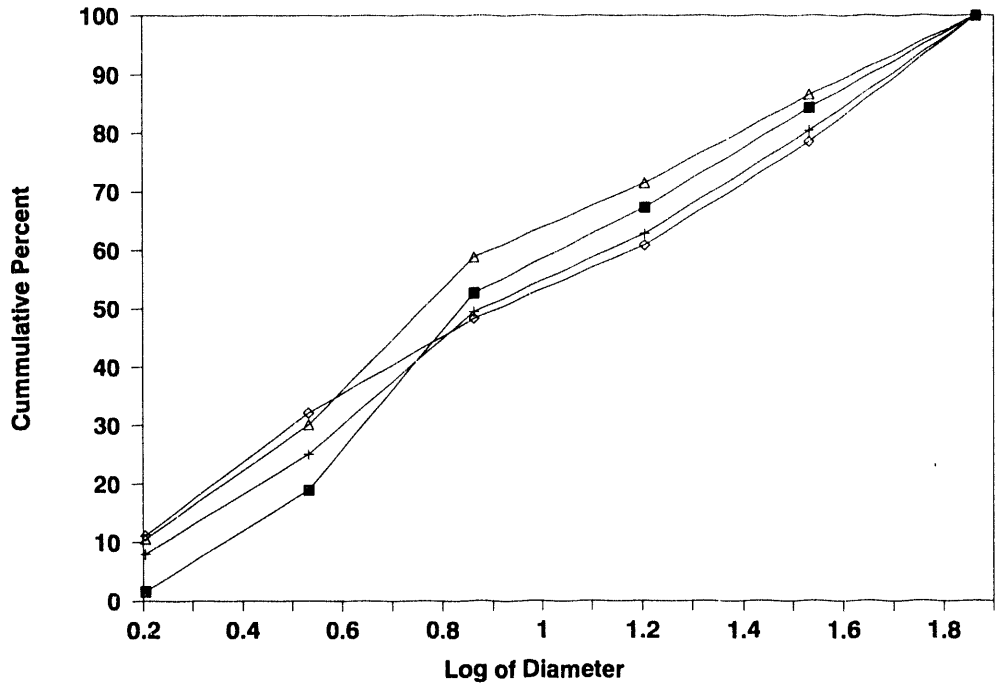

Figure 4. Cumulative percent minerals versus size for Beulah coal minerals.

smallest size bin, the major error lies in the range of particles that will have the largest impact because of the log scale (volume is proportional to the radius cubed) and magnifications used. The error in the small range is most likely due to the step size of the analysis which is slightly over one micron, and the fact that the beam diameter is one micron and the sampling volume approximately 3 microns. The previous error may be remedied by the addition of a higher magnification to detect smaller particles. The one problem with looking at small particles is that in order to decrease the diameter of the beam, the current used must be decreased. Decreased beam current also causes the contrast produced in the backscatter mode to decrease, which is an undesired effect.

Table 3 is a more elaborate breakdown of the differences between four runs on the same coal mounted in carnauba wax. The total deviation of the analysis is 33.4 (out of 100), and this would correspond to a 45% confidence limit on the numbers. A ninety percent confidence limit would allow for an error of up to approximately 65% change in the total analysis.

Table 4 is the particle-size distribution of the carnauba wax sample. Figure 5 is the cumulative distribution of the same. This data is very similar to the particle-size data addressed earlier.

The third study looked at the analysis of one frame on the Beulah sample five times. All five analyses were done back-to-back, with all beam parameters and thresholds checked before and after each analysis. The first

TABLE 3

BEULAH STANDARD (EXCL. OVER) WT% BASIS OVERALL
CARNAUBA WAX MOUNT

	RUN #1	RUN #2	RUN #3	RUN #6	AVG	STD DEV. (S^2/4)^.5	% ERROR
Quartz	6.8	5.3	19.8	5.5	9.3	7.0	64.8
Iron Oxide	2.7	1.1	0.3	1.1	1.3	1.0	69.4
Aluminosilicate	27.4	21.1	27.0	29.6	26.3	3.6	12.0
Ca-Aluminosilicate	0.9	0.5	1.4	2.7	1.4	1.0	59.8
Fe-Aluminosilicate	0.5	1.5	1.1	1.8	1.2	0.5	39.7
K-Aluminosilicate	1.0	0.6	3.5	2.1	1.8	1.1	63.6
Ankerite	0.0	0.0	0.0	0.0	0.0	0.0	0.0
Pyrite	11.5	15.1	15.7	8.8	12.8	2.8	21.9
Gypsum	23.3	13.1	15.6	17.4	17.3	4.3	21.6
Barite	3.6	3.1	1.6	4.0	3.1	0.9	29.7
Gypsum/Barite	1.3	0.2	0.2	0.3	0.5	0.5	93.9
Apatite	0.0	0.0	0.0	0.0	0.0	0.0	0.0
Ca-Silicate	0.1	0.1	0.2	0.1	0.1	0.0	14.0
Gyp/Aluminosilicate	0.0	0.3	0.1	1.1	0.4	0.4	110.4
Ca-Aluminate	0.0	0.0	0.0	0.0	0.0	0.0	0.0
Spinel	0.0	0.0	0.0	0.0	0.0	0.0	0.0
Alumina	0.0	0.5	0.3	0.0	0.2	0.2	105.9
Calcite	0.6	0.0	0.0	0.1	0.2	0.2	127.0
Rutile	0.3	0.3	1.2	0.1	0.5	0.4	86.4
Dolomite	0.0	0.0	0.0	0.0	0.0	0.0	0.0
Pyrrhotite	9.5	24.9	6.1	8.5	12.2	8.6	60.3
Ca-Rich	0.0	0.0	0.0	0.0	0.0	0.0	0.0
Si-Rich	0.2	0.4	1.1	1.1	0.7	0.4	58.2
Periclase	0.0	0.0	0.0	0.0	0.0	0.0	0.0
Unknown	10.4	11.8	4.9	15.6	10.7	3.8	35.8
	100.0	100.0	100.0	100.0	100.0	33.4	AVG 43.0

TABLE 4

BEULAH LIGNITE PARTICLE-SIZE DISTRIBUTION
CARNAUBA WAX

Size Bin (μm)	Test #1	Test #2	Test #3	Test #4	Average	Deviation	% Error
1 to 2.2	1.64	7.95	11.13	10.57	7.82	3.37	43.08
2.2 to 4.6	17.32	17.06	20.93	19.50	18.70	1.43	7.65
4.6 to 10.0	33.71	24.36	16.17	28.68	25.73	7.40	22.36
10.0 to 22.0	17.06	13.37	12.53	12.67	13.30	0.74	5.57
22.0 to 46.0	17.06	17.68	17.73	15.09	16.89	0.96	5.6
46.0 to 100.0	15.66	19.59	21.50	13.49	17.56	3.60	16.07

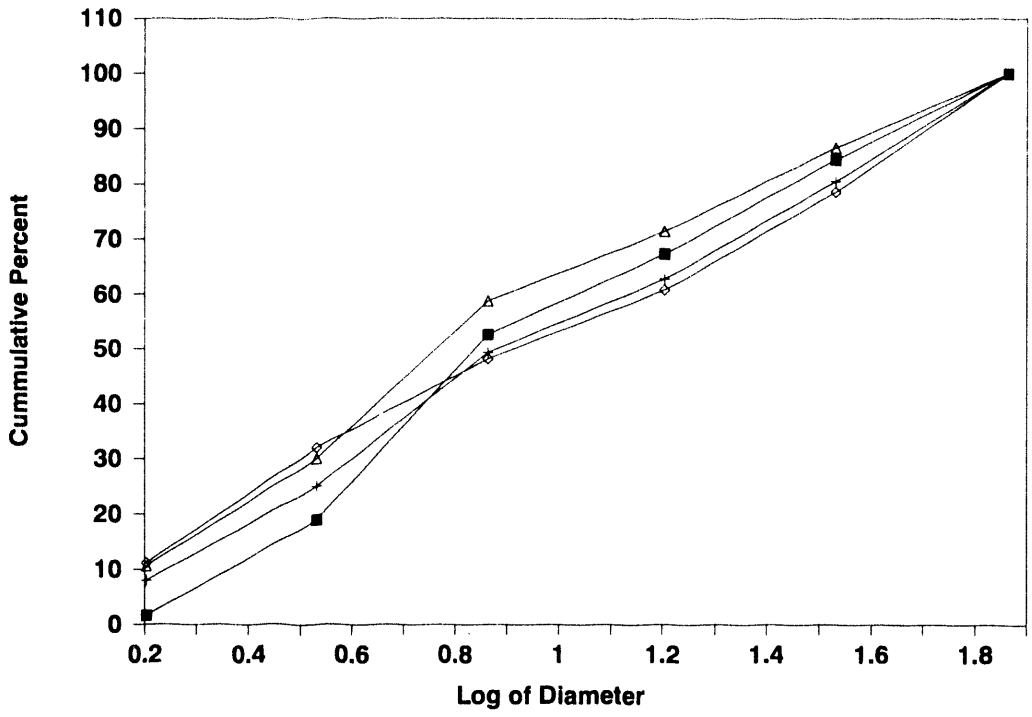

Figure 5. Cumulative size distribution of Beulah minerals mounted in carnauba wax mounting medium.

100 particles found were all that were looked at. Only 19 out of the 100 were found all five times, with 7 found four out of five times, and 44 only found once. The results are in Table 5. Even when the particles were found more than once, there was often a difference in the area recorded. When the particles were found all five times, there was a 13.9% error in the area recorded. A major parameter currently being tested is the length of the dwell time during analysis. The dwell time is the amount of time spent recording the backscatter electron intensity signal. A longer signal may alleviate much of the error seen in this analysis.

2.2.1 Proposed Changes to Present Analysis

Based on the above findings, we are going to implement the following changes to the present CCSEM analysis:

1) We are going to go to three magnifications (instead of the present two magnifications) to reduce error and increase the utility of the digital images.

2) We are going to increase the video signal, as we have found that this increases our reproducibility.

3) We are going to implement a new Fortran program (described below in the CCSEM automation and development section).

TABLE 5

FIVE-FRAME TEST
BEULAH

Number of Times Found	Number of Particles	Average % Error in Area
5	19	13.9
4	7	16.35
3	11	10.33
2	19	26.9
1	44	--
	100	

It is hoped that these changes will increase the reproducibility of the present analysis, increasing the utility of the technique. In a further effort to elucidate the utility and validity of the technique, a round-robin of samples tested at EERC is presently being organized. Researchers chosen for the initial round-robin include Dr. W. Strazheim, Ames Laboratory; Dr. J. Huffman, University of Kentucky; Mr. M. Farrell, CANMET; Dr. L. Baxter and Dr. F. Gruelich, Sandia National Laboratories; Dr. G. Casuccio, R.J. Lee Group; Mr. D. Elegy, Pacific Northwest Laboratories; Dr. G. Hamburg, Netherlands Energy Research Foundation ECN; Mr. Paul Gottlieb, CSIRO; Mr. Peter Solomon, Advanced Fuel Research, Inc. These researchers were contacted with a questionnaire concerning the logistics of the round-robin. It is hoped that the round-robin will proceed by December 31, 1990.

2.3 Subtask B: CCSEM Automation and Development

2.3.1 CCSEM Automation

Work in the area of CCSEM automation and development has focused on the automation of the present analysis and establishing an interface allowing transfer of CCSEM field areas to the image analysis system for automated image collection and storage. Both of these tasks have now been completed.

The CCSEM automation allows the analysis to be run unattended and expands the practical numerical limits of the analysis. A further advantage of the automation is better control on the area covered; this is because the area covered is saved to disk and preset by the operator.

Modifications to the present CCSEM program will allow for simultaneous image acquisition and produce additional data concerning the relationship of the mineral grains to the coal matrix as well as any mineral associations present. The present method used to determine the juxtaposition of the coal mineral matter involves the standard CCSEM analysis of the coal. However, prior to the analysis of each frame examined, a backscattered image is

obtained and saved to the TN8500 image analysis system. As the CCSEM analysis proceeds, each particle analyzed is identified on the image. The data can be modified to include juxtapositional relationships.

2.3.2 Relationship of Surface Area to Volume in CCSEM Analysis

Some questions were raised at the DOE Mineral Transformations Project Review Meeting in Tucson about the relationship between the area fraction of a phase determined by CCSEM and the volume fraction of that phase. The basic equivalence of the area fraction and the volume fraction was worked out by A. Delesse, a French petrographer, in 1848, so the following basic development is far from new.

To find the average value of x from a series of measurements of x, the values found by each individual measurement are summed, then divided by the total number of measurements. A more useful way of defining the average value of a series of measurements is to group them and then add them. For example, if n_i is the number of times that x takes on the value x_i, then

$$x_{avg} = \Sigma\ (x_i)(n_i)/n \qquad \text{[Eq. 1]}$$

where n is the total number of measurements. However, n_i/n is the frequency of the occurrence of x_i, designated $f(x_i)$. Therefore, the average value of x can be written

$$x_{avg} = \Sigma\ (x_i)f(x_i) \qquad \text{[Eq. 2]}$$

For a continuous function, the definition is:

$$x_{avg} = \int_{-\infty}^{\infty} x\ f(x)\ dx \qquad \text{[Eq. 3]}$$

As an example, because CCSEM analysis measures the area of phases exposed at the surface of a cross section, we will calculate the average area of an exposed cross section of a sphere that has been sliced along parallel planes. Statisticians often call the average in such a situation the "expected" value of the area of the cross section. For this example, we will use the simplified system of a sphere of radius R, composed of phase A, contained in a cube of sides 2R, and composed of phase B as shown in Figure 6. If the cube is cross-sectioned along planes parallel to the base, then the sphere is also sectioned. The radius of the section will be designated r(z) since the length of r is a function of z, the height at which the cube was sectioned.

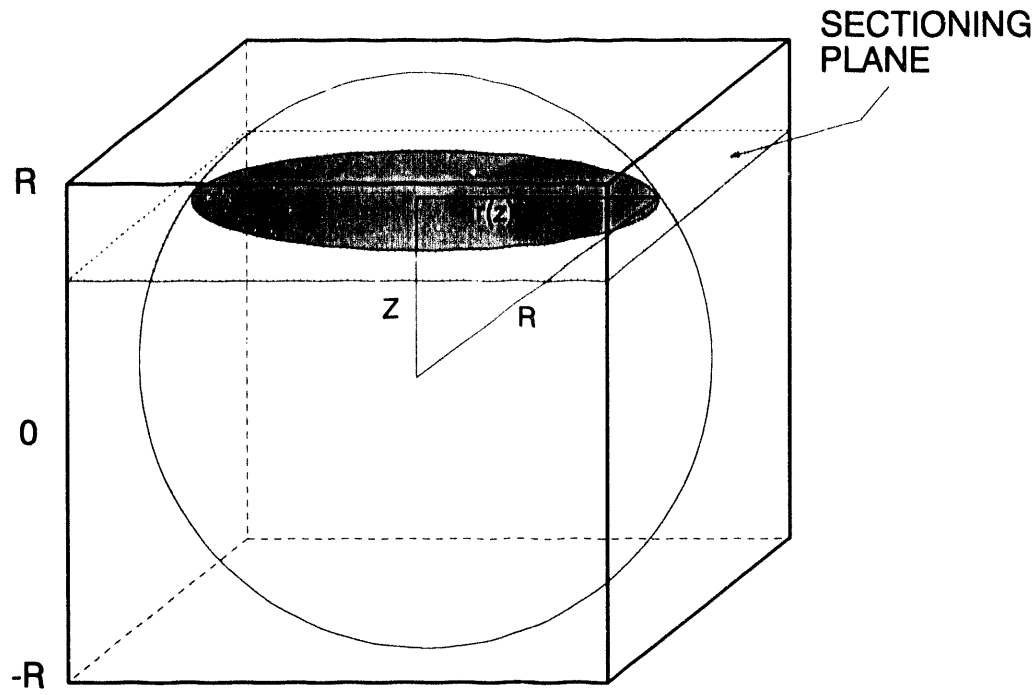

Figure 6. Relation of surface area to volume for spherical particles that are cross-sectioned.

The average or expected area of the cross section is:

$$A_{avg} = A(z)\ f(z)\ dz \qquad \text{[Eq. 4]}$$

where f(z) dz is the probability of sectioning between z and z+dz. For a homogeneous sphere of diameter 2R and a random cross section, the frequency of intersection at a given z is:

$$f(z)\ dz = dz/2R \qquad \text{[Eq. 5]}$$

Also, the area of the exposed cross section at a height z is:

$$A(z) = \pi\ r^2(z) \qquad \text{[Eq. 6]}$$

where:

$$r^2 = R^2 - z^2 \qquad \text{[Eq. 7]}$$

Substituting yields:

$$A_{avg} = \pi (R^2 - z^2)\, dz / 2R \qquad \text{[Eq. 8]}$$
$$= 2\pi R^2/3$$

It is tempting to think that the average cross-section area is 2/3 of the "actual" or "true" cross-sectional area. This is an incorrect way of thinking of the average area of cross-sections produced along parallel planes. In fact, the average area is 2/3 of the maximum possible cross-sectional area, not 2/3 of the "actual" area. In general, the area that best characterizes the cross sections of a sphere produced along parallel planes is the average or expected area as calculated above. However, the relationship between the expected value of a parameter (area, diameter, etc.) and the maximum value can be used to correct for sectioning in distribution curves.

Another misconception is that because the average area of a cross section produced along parallel planes is 2/3 of the maximum, then the volume fraction of the phase, calculated from measured area fractions, must be 2/3 of the true volume fraction. This supposition is non sequitur; i.e., the first relationship cannot be logically extended to the second relationship. As an example of the relationship between the average area fraction and the volume fraction, we can refer again to the situation shown in Figure 6. The total area of a cross section of the cube (including the sphere) oriented parallel to a face is always $4R^2$. The expected average area of the sphere sectioned in a similar manner is, as shown above, $2\pi R^2/3$. The ratio of the expected, or average area of the exposed cross section of the sphere to that of the total area is then given by:

$$\text{Area of Sphere Cross Section/Total Area} = (2\pi R^2/3) / 4R^2 \qquad \text{[Eq. 9]}$$
$$= \pi/6$$

The volume ratio is given by:

$$\text{Volume of Sphere/Total Volume of Cube} = (4\pi R^3/3) / 8R^3 \qquad \text{[Eq. 10]}$$
$$= \pi/6$$

Thus, for this example, the ratio of the average area of the cross section of a sphere to the total area analyzed is equal to the ratio of the volume of the sphere to the volume of the sample; i.e., the average area fraction equals the volume fraction.

The situation encountered during CCSEM analysis is, of course, more complicated. However, Delesse proved the general case of the equivalence of average area fraction and volume fraction in 1848. The proof of the general case was modified to better reflect the situation we encounter during CCSEM

analysis. Much of the following development was taken from the writings of J.E. Hilliard as presented in Quantitative Microscopy (7).

A more general situation encountered during CCSEM analysis of minerals in coal is depicted in Figure 7. The total volume of the sample is that of the cylindrical SEM plug of radius R and height H. The A phase is composed of many, irregular particles distributed throughout the plug.

For any given height z above the base, the fraction of the total exposed area that is occupied by the A phase is given by:

$$\alpha_A(z) = A_A(z) \; / \; \pi R^2 \qquad \text{[Eq. 11]}$$

where: $\alpha_A(z)$ = the area fraction of phase A
$A_A(z)$ = the area of phase A exposed by the section

The average area fraction of A is:

$$\text{Average } \alpha_A = \alpha_A(z) \; f(z) \; dz \qquad \text{[Eq. 12]}$$

where f(z) dz is the probability that the section occurs between z and z + dz. For a truly random cross section, the probability of sectioning at a height z is the same as the probability for sectioning at any other height and is given by:

$$f(z) \; dz = dz \; / \; H \qquad \text{[Eq. 13]}$$

Substituting this relationship and the definition for area fraction yields:

$$\text{Average } \alpha_A = A_A(z) \; dz \; / \; \pi R^2 H \qquad \text{[Eq. 14]}$$

The numerator of this fraction is, by definition, equal to the volume of phase A in the plug, while the denominator is equal to the volume of the plug. In other words, in the general case, the average area fraction of a phase exposed at a cross section of a homogeneous sample is equal to the volume fraction of that phase.

2.3.3 Graphic Output of CCSEM Analysis

One of the problems with the present CCSEM analysis is that the output can be difficult to interpret by virtue of its complexity. Since it provides size, shape, juxtaposition, mineralogy, and inherent/extraneous information, the volume of data can be difficult to handle. For this reason, one of the

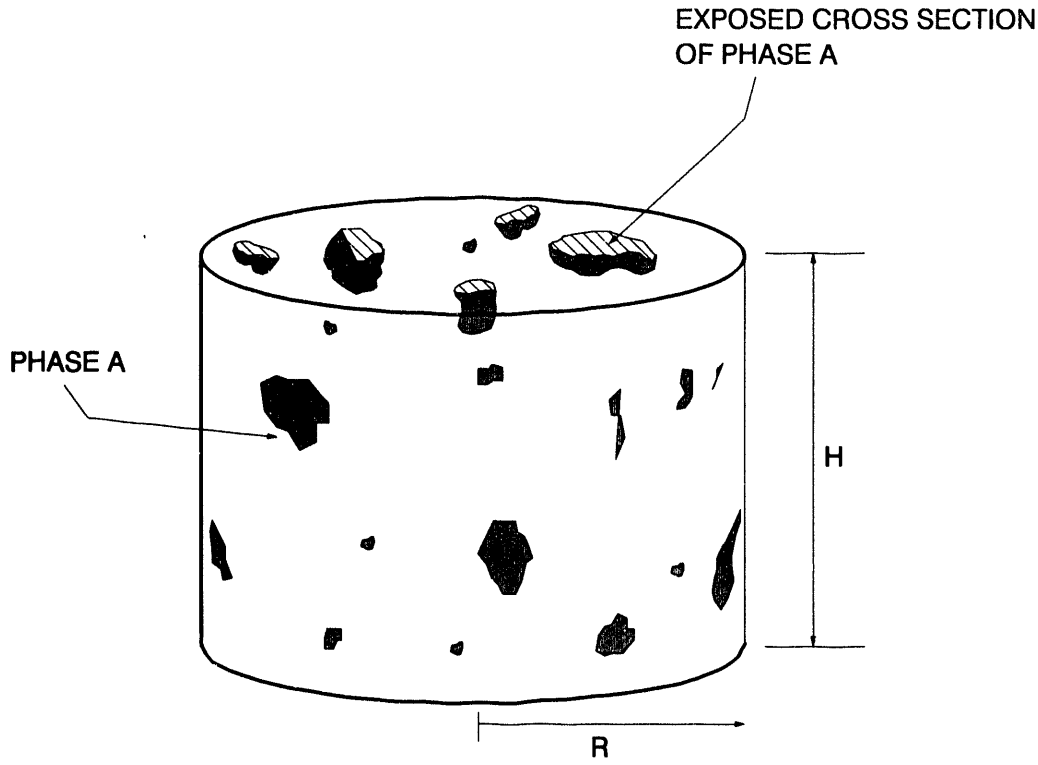

Figure 7. Typical cross-sectioned cast of epoxy-coal for SEM analysis.

objectives of this project is to work towards more standardized, graphic outputs designed to ease the interpretation of the data. The intent is that once fully developed, these graphic outputs will be added to the data manipulation program as standard outputs.

Figure 8 shows an example of one type of graph we are presently using to display the particle-size evolution during combustion using CCSEM data. Figure 9 shows an example of a graphical representation of mineral composition data from CCSEM analysis. Another type of graphical presentation of CCSEM mineral data is a ternary plot of elemental components of the particles analyzed using CCSEM. Figure 10a is a ternary plot of Eagle Butte coal mineral data and Figure 10b is a plot of fly ash data where Si, Al, and Ca were used as the apices of the ternary plots. These types of plots reveal interaction between elemental components in coal minerals during combustion.

2.3.4 Improved Fortran Data Manipulation Program

The program to determine mineral phases and to distribute the particles into size bins using CCSEM data has been changed in such a way as to facilitate future modifications and to improve the organization and documentation. Mineral phases have also been added to provide a more fully quantitative set of phases by reducing the unknowns. Along with the addition of these phases, the definitions of previously used phases have been restructured to further

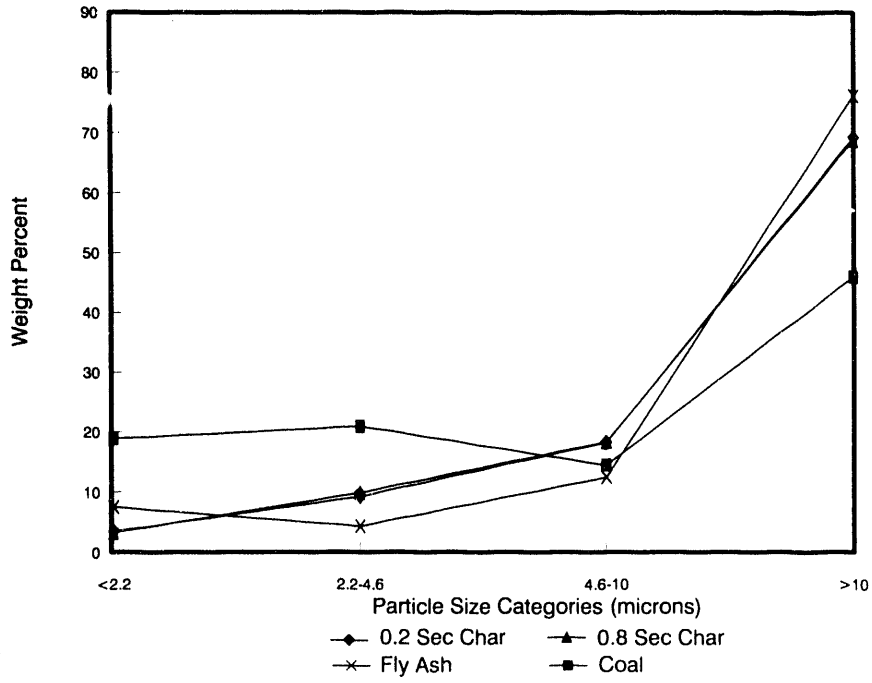

Figure 8. Example graph of particle-size evolution during combustion of Beulah coal as derived from CCSEM analysis.

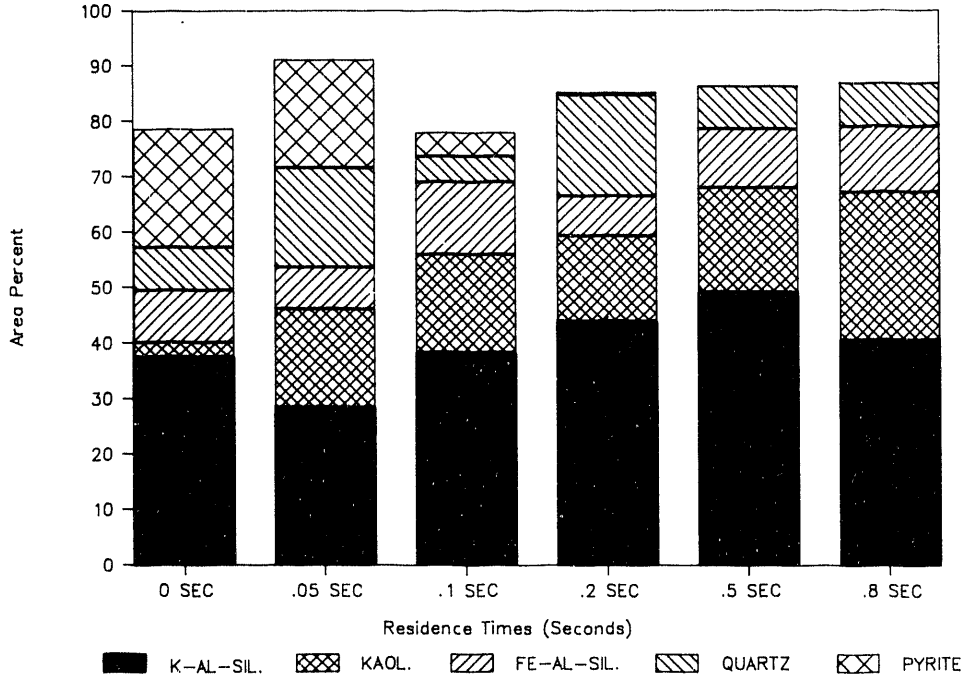

Figure 9. Graphical representation of CCSEM inorganic phases in Upper Freeport coal and char samples as a function of residence time in a DTF combustor.

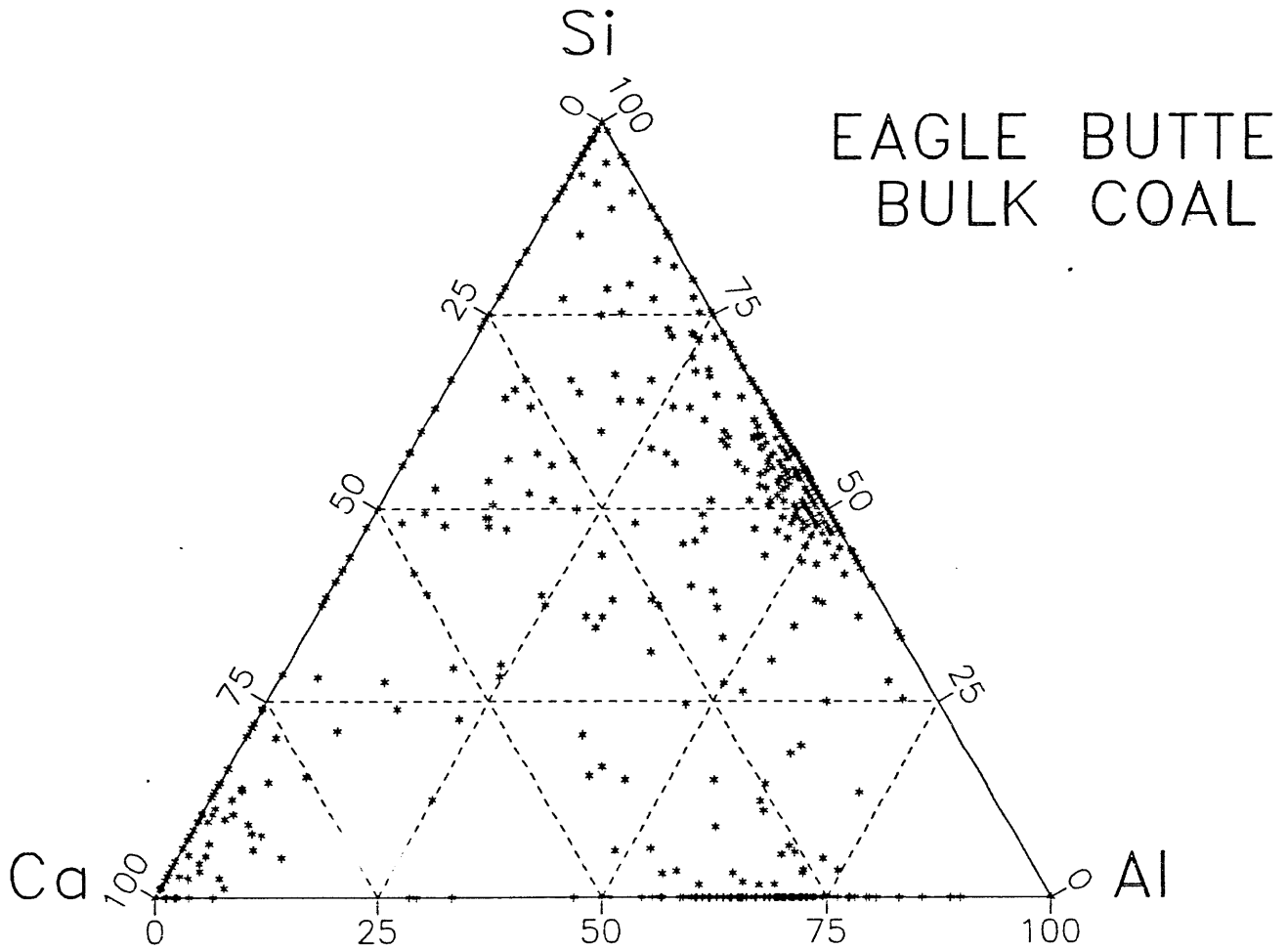

Figure 10a. Ternary plot of Ca, Al, and Si content in Eagle Butte mineral particles as analyzed using CCSEM.

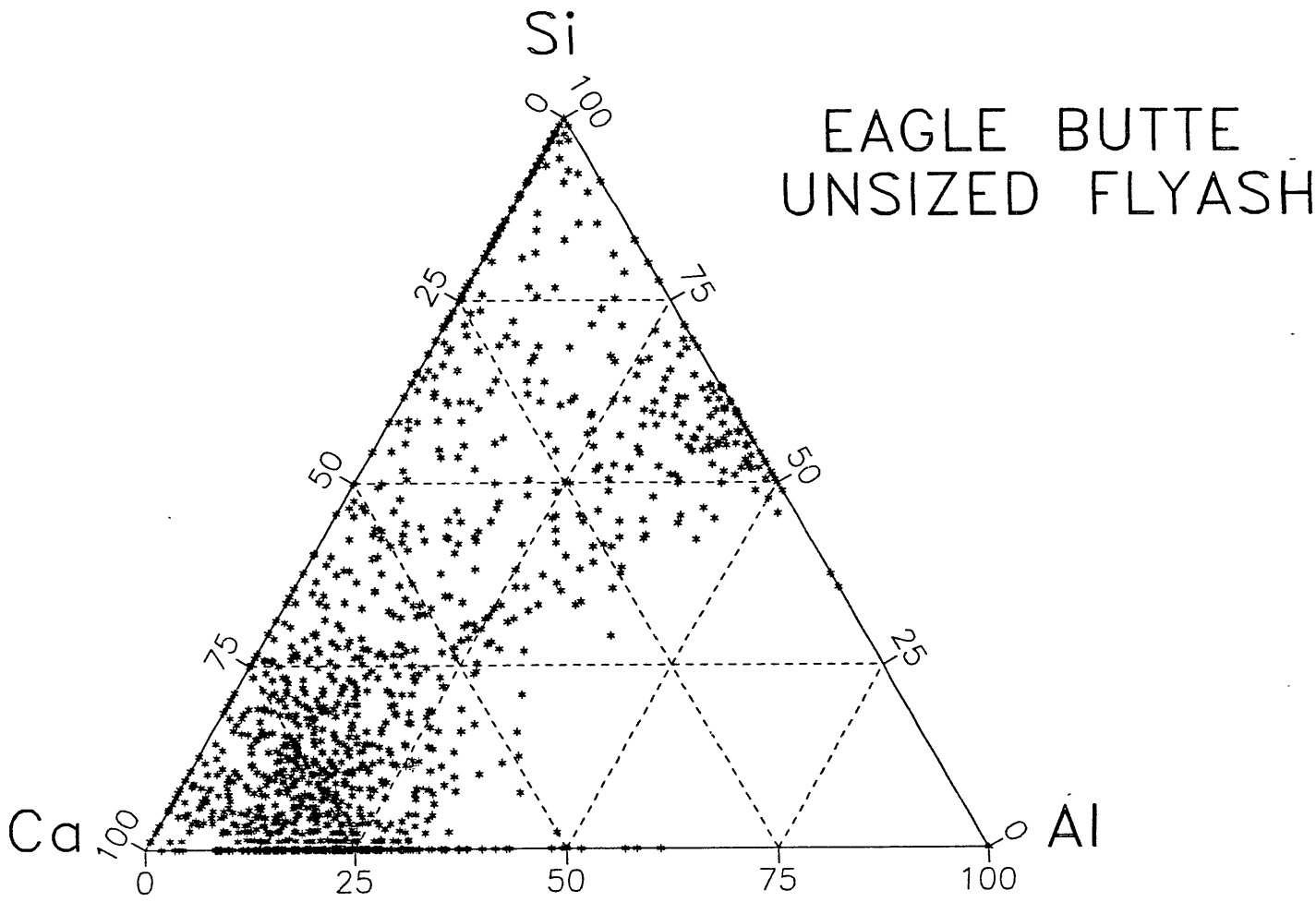

Figure 10b. Ternary plot of Ca, Al, and Si content in Eagle Butte fly ash particles as analyzed using CCSEM.

reduce error in the classifications. The tightening of phase definitions was accomplished using our experience in the analysis of coal, char, and fly ash minerals. Because of the improved readability and structure of the program, improving and changing phase definitions in the future will be more easily accomplished. Table 6 lists the criteria for classifying the 31 minerals and phases included in the updated CCSEM program. The program also no longer depends upon the magnifications and guard regions for the analysis to remain static, but allows for the user to input these and then calculates the needed information from them. The actual output has also been cleaned up by adding a one-page, quick summary and by formatting the entire output to provide greater readability for the user. In the past, it has been noticed that the CCSEM program on the Tracor Northern system would find particles slightly larger than the specified sizes. Since two magnifications are run on the same area, with the maximum particle size of the higher magnification being the minimum size of the lower magnification, the same particle was being identified twice, once at each magnification. This has been compensated for by discarding particles above the maximum size range for each particular magnification. Table 7 lists an example of the output from the new Fortran program.

2.3.5 Planned Developments

In all, however, the present technique is not an acceptable analysis for the final output of this research effort. The present technique relies on the combination of analog signal and digital imaging techniques but doesn't allow for the coal and mineral particle-by-particle analysis needed to achieve our goals. In order to achieve the particle-by-particle type of analysis, a new technique was conceived which will give the needed data and potentially increase the accuracy of the chemical and sizing analysis as well.

The proposed method will use the integrated imaging and EDS analysis to simultaneously investigate the detailed morphologic and chemical data present in the coal and mineral particles. The program will first collect a digital image from a polished cross section of pulverized coal and mineral sample. The coal, minerals, and mounting media will be separated into phases based on differences in grey level intensities present in the backscattered image. The relative brightness of the mineral phases will be used to create a binary image. This binary image will be used to control the electron beam to collect EDS spectral information for each point. The chemistries of the mineral phases will be determined using the EDS spectral information. The differing grey levels present will be used to indicate the relationship of the mineral phases to the parent coal and to one another. Since each phase will be assigned to individual pixels, the program will be able to produce boundary data for each phase present. The number of pixels shared by each phase with each other and the coal will be calculated and determinations made about the associations present. These analyses will result in a map of the chemistry of each field along with the morphologic information concerning the relationship of minerals to one another and to the coal matrix. Figure 11 shows the type of information that will be produced.

TABLE 6

CRITERIA FOR CLASSIFYING MINERALS AND INORGANIC PHASES USING CCSEM

Mineral Name	Criteria	Density
Quartz	Al<=5, Si>=80	2.65
Iron Oxide	Si<10, S<=5, Mg<=5, Al<=5, Fe>=80	5.30
Periclase	Mg>=80, Ca<=5	3.61
Rutile	S<=5, Ti + Ba>=80	4.90
Alumina	Al>=80	4.00
Calcite	S<10, Mg<=5, Si<=5, P<=5, Ti<=5, Ba<=5, Ca>=80	2.80
Dolomite	Mg=>5, Ca>10, Ca + Mg>=80	2.86
Ankerite	S<15, Mg<Fe, Fe>20, Ca>20, Ca + Mg + Fe>=80	3.00
Kaolinite	Al + Si>=80, 0.8< Si/Al <1.5, Fe<=5, K<=5, Ca<=5	2.65
Montmorillonite	Al + Si>=80, 1.5< Si/Al <2.5, Fe<=5, K<=5, Ca<=5	2.50
K-Al-Silicate	Na<=5, Ca<=5, Fe<=5, K=>5, Si>20, Al=>15, K + Al + Si>=80	2.60
Fe-Al-Silicate	Fe=>5, Al=>15, Si>20, S=<5, Ca<=5, K<=5, Na=<5, Fe + Al + Si>=80	2.80
Ca-Al-Silicate	S<=5, K<=5, Fe<=5, Na<=5, Ca=>5, Al=>15, Si>20, Ca + Al + Si>=80	2.65
Na-Al-Silicate	S<=5, K<=5, Fe<=5, Ca<=5, Na=>5, Al=>15, Si>20, Na + Al + Si>=80	2.60
Aluminosilicate	K<=5, Ca<=5, Fe<=5, Na<=5, Si>20, Al>20, Si + Al>=80	2.65
Mixed Silicates	Na<10, Fe<10, Ca<10, K<10, S<=5, Si>20, Al>20, Si + Al + Fe + Ca + K + Na>=80	2.65
Fe-Silicate	Fe>10, Na<=5, K<=5, Ca<=5, Al<=5, S<=5, Si>20, Fe + Si>=80	4.40
Ca-Silicate	Na<=5, K<=5, Fe<=5, Al<=5, S<=5, Ca>10, Si>20, Ca + Si>=80	3.09
Ca-Aluminate	P<=5, S<=5, Si<=5, Al>15, Ca>20, Ca + Al>=80	2.80
Pyrite	Ca<10, 10<= Fe =<40, S>40, Fe + S>=80	5.00
Pyrrhotite	10=< S <40, Fe<40, Fe + S>=80	4.60
Gypsum	Ti<10, Ba<10, Si<10, S>20, Ca>20, Ca + S>=80	2.50
Barite	Fe<10, Ca<=5, S>20, Ba + Ti>20, Ba + S + Ti>=80	4.50
Apatite	P>=20, Ca>=20, Al<=5, S<=5, Ca + P>=80	3.20
Ca-Al-P	Al>10, P>10, Ca>10, S<=5, Si<=5, Al + Ca + P>=80	2.80
KCl	K>=30, CL>=30, K + CL>=80	1.99
Gypsum/Barite	Fe<=5, Ca=>5, Ba=>5, Ti=>5, S>20, Ca + Ba + S + Ti>=80	3.50
Gypsum/Al-Sil.	Al=>5, Si=>5, S=>5, Ca=>5, Ca + Al+ Si + S>=80	2.60
Si-Rich	65<= Si <80	2.65
Ca-Rich	65<= Ca <80, Al<15	2.60
Unknown	All Other Compositions	2.70

TABLE 7

EXAMPLE TEST PAGES

EXAMPLE TEST PAGE 1

Summary of CCSEM Results: Prog Version 1BF 5/21/90

Sample Description ---> Example Test
Submitter ---> John Doe
ICC # and Fund # ---> 49330978

Summary of Parameters

Percent Epoxy Used	=	0.0
Total Mineral Area Analyzed at High Mag	=	10176.3
Normalized Area Analyzed at High Mag	=	732512.4
Total Mineral Area Analyzed at Low Mag	=	86719.4
Field Size Used at High Mag	=	115519.773
Field Size Used at Low Mag	=	2494610.477
Number of Frames at High Mag	=	6
Number of Frames at Low Mag	=	20
Total Mineral Area on a Coal Basis	=	1.642
Total Mineral Wt% on a Coal Basis	=	3.217
Total Number of Points Analyzed	=	1552
Number of Points Under Threshold	=	48

Weight Percent on a Mineral Basis

	1.0 to 2.2	2.2 to 4.6	4.6 to 10.0	10.0 to 22.0	22.0 to 46.0	46.0 to 100.0	TOTALS
Quartz	.2	.9	1.0	.8	.7	.7	4.4
Iron Oxide	.0	.0	.0	.0	.0	.0	.1
Periclase	.0	.0	.0	.0	.0	.0	.0
Rutile	.0	.0	.0	.0	.0	.0	.0
Alumina	.0	.0	.0	.0	.0	.0	.0
Calcite	.0	.0	.0	.0	.0	.0	.0
Dolomite	.0	.0	.0	.0	.0	.0	.0
Ankerite	.0	.0	.0	.0	.0	.0	.0
Kaolinite	.0	.0	.0	.2	.1	.0	.3
Montmorillonite	.1	.0	.0	.1	.2	.0	.4
K-Al-Silicate	.1	.0	.0	.2	.1	.3	.6
Fe-Al-Silicate	.0	.1	.0	.0	.0	.0	.1
Ca-Al-Silicate	.0	.1	.0	.0	.0	.0	.2
Na-Al-Silicate	.0	.0	.0	.0	.0	.0	.0
Aluminosilicate	.0	.0	.0	.0	.0	.0	.1
Mixed Silicates	.0	.1	.0	.0	.0	.0	.1
Fe Silicate	.0	.0	.0	.0	.0	.0	.0

continued . . .

TABLE 7 (Continued)

EXAMPLE TEST PAGES

	1.0 to 2.2	2.2 to 4.6	4.6 to 10.0	10.0 to 22.0	22.0 to 46.0	46.0 to 100.0	TOTALS
Ca-Silicate	.0	.0	.0	.0	.0	.0	.0
Ca-Aluminate	.1	.C	.0	.0	.0	.0	.1
Pyrite	.1	.0	.0	.4	1.0	1.9	3.4
Pyrrhotite	.0	.0	.0	.0	.0	.0	.0
Gypsum	.0	.0	.0	.0	.0	.0	.0
Barite	.1	.0	.0	.2	.0	.0	.2
Apatite	.0	.0	.0	.0	.0	.0	.0
Ca-Al-P	3.0	14.6	24.2	2.0	.2	.3	44.3
KCl	.0	.0	.0	.0	.0	.0	.0
Gypsum/Barite	.0	.1	.2	.0	.0	.0	.3
Gypsum/Al-Silic	.0	.0	.0	.0	.0	.0	.0
Si-Rich	.1	.0	.0	.2	.2	.7	1.3
Ca-Rich	.1	.3	.2	.0	.0	.0	.7
Unknown	9.5	18.1	14.8	.8	.3	.0	43.5
Totals	13.6	34.2	40.4	5.0	3.0	3.9	100.0

EXAMPLE TEST PAGE 2

Area in Each Size Range

	1.0 to 2.2	2.2 to 4.6	4.6 to 10.0	10.0 to 22.0	22.0 to 46.0	46.0 to 100.0	TOTALS
Quartz	28.2	107.6	118.2	7305.9	5954.9	6077.7	19592.5
Iron Oxide	2.4	.0	.0	108.7	.0	.0	111.0
Periclase	.0	.0	.0	.0	.0	.0	.0
Rutile	.0	.0	.0	.0	.0	.0	.0
Alumina	.0	.0	.0	.0	.0	.0	.0
Calcite	1.5	.0	.0	.0	.0	.0	1.5
Dolomite	.0	.0	.0	.0	.0	.0	.0
Ankerite	.0	.0	.0	.0	.0	.0	.0
Kaolinite	.0	.0	.0	1519.4	1229.7	.0	2749.1
Montmorillonite	7.9	3.9	.0	1035.3	2039.6	.0	3086.7
K-Al-Silicate	7.4	.0	.0	1604.9	986.2	2334.0	4932.4
Fe-Al-Silicate	.0	10.1	.0	.0	.0	.0	10.1
Ca-Al-Silicate	4.2	15.3	.0	.0	.0	.0	19.6
Na-Al-Silicate	.0	.0	.0	.0	.0	.0	.0
Aluminosilicate	3.7	.0	.0	338.5	427.3	.0	769.4

continued . . .

TABLE 7 (Continued)

EXAMPLE TEST PAGES

	1.0 to 2.2	2.2 to 4.6	4.6 to 10.0	10.0 to 22.0	22.0 to 46.0	46.0 to 100.0	TOTALS
Mixed Silicates	.0	7.7	.0	.0	.0	.0	7.7
Fe-Silicate	.0	.0	.0	.0	.0	.0	.0
Ca-Silicate	3.9	.0	.0	.0	.0	.0	3.9
Ca-Aluminate	7.4	.0	.0	.0	.0	.0	7.4
Pyrite	4.8	.0	.0	1806.1	4567.4	8646.6	15024.8
Pyrrhotite	.0	.0	.0	.0	.0	.0	.0
Gypsum	4.1	.0	.0	.0	.0	.0	4.1
Barite	3.7	.0	.0	947.8	.0	.0	951.5
Apatite	.0	.0	.0	.0	.0	.0	.0
Ca-Al-P	344.1	1650.5	2738.4	16067.8	1853.5	2314.5	24968.8
KCl	.0	.0	.0	.0	.0	.0	.0
Gypsum/Barite	2.8	6.7	17.9	.0	.0	.0	27.3
Gypsum/Al-Silic	3.8	.0	.0	.0	.0	.0	3.8
Si-Rich	9.6	.0	.0	2002.6	1857.2	6358.7	10228.1
Ca-Rich	16.5	38.6	25.0	.0	.0	.0	80.0
Unknown	1116.6	2122.4	1741.5	6840.3	2495.1	.0	14315.9
Totals	1572.6	3962.8	4640.9	39577.0	21410.9	25731.5	96895.7

EXAMPLE TEST PAGE 3

Normalized Area in Each Size Range

	1.0 to 2.2	2.2 to 4.6	4.6 to 10.0	10.0 to 22.0	22.0 to 46.0	46.0 to 100.0	TOTALS
Quartz	2030.6	7743.8	8507.6	7305.9	5954.9	6077.7	37620.6
Iron Oxide	171.3	.0	.0	108.7	.0	.0	280.0
Periclase	.0	.0	.0	.0	.0	.0	.0
Rutile	.0	.0	.0	.0	.0	.0	.0
Alumina	.0	.0	.0	.0	.0	.0	.0
Calcite	107.3	.0	.0	.0	.0	.0	107.3
Dolomite	.0	.0	.0	.0	.0	.0	.0
Ankerite	.0	.0	.0	.0	.0	.0	.0
Kaolinite	.0	.0	.0	1519.4	1229.7	.0	2749.1
Montmorillonite	571.5	280.7	.0	1035.3	2039.6	.0	3927.1
K-Al-Silicate	532.7	.0	.0	1604.9	986.2	2334.0	5457.7
Fe-Al-Silicate	.0	727.0	.0	.0	.0	.0	727.0
Ca-Al-Silicate	305.2	1102.8	.0	.0	.0	.0	1408.0

continued . . .

TABLE 7 (Continued)

EXAMPLE TEST PAGES

	1.0 to 2.2	2.2 to 4.6	4.6 to 10.0	10.0 to 22.0	22.0 to 46.0	46.0 to 100.0	TOTALS
Na-Al-Silicate	.0	.0	.0	.0	.0	.0	.0
Aluminosilicate	264.9	.0	.0	338.5	427.3	.0	1030.7
Mixed Silicates	.0	552.8	.0	.0	.0	.0	552.8
Fe-Silicate	.0	.0	.0	.0	.0	.0	.0
Ca-Silicate	283.6	.0	.0	.0	.0	.0	283.6
Ca-Aluminate	529.8	.0	.0	.0	.0	.0	529.8
Pyrite	344.8	.0	.0	1806.1	4567.4	8646.6	15364.8
Pyrrhotite	.0	.0	.0	.0	.0	.0	.0
Gypsum	293.0	.0	.0	.0	.0	.0	293.0
Barite	269.2	.0	.0	947.8	.0	.0	1217.0
Apatite	.0	.0	.0	.0	.0	.0	.0
Ca-Al-P	24769.8	118809.5	197115.3	16067.8	1853.5	2314.5	360930.3
KCl	.0	.0	.0	.0	.0	.0	.0
Gypsum/Barite	199.4	480.8	1287.0	.0	.0	.0	1967.3
Gypsum/Al-Silic	274.3	.0	.0	.0	.0	.0	274.3
Si-Rich	692.5	.0	.0	2002.6	1857.2	6358.7	10910.9
Ca-Rich	1186.3	2776.4	1797.4	.0	.0	.0	5760.0
Unknown	80373.9	152775.0	125356.3	6840.3	2495.1	.0	367840.7
Totals	113200.0	285248.9	334063.6	39577.0	21410.9	25731.5	819231.9

Area Percent Mineral Basis

	1.0 to 2.2	2.2 to 4.6	4.6 to 10.0	10.0 to 22.0	22.0 to 46.0	46.0 to 100.0	TOTALS
Quartz	.2	.9	1.0	.9	.7	.7	4.6
Iron Oxide	.0	.0	.0	.0	.0	.0	.0
Periclase	.0	.0	.0	.0	.0	.0	.0
Rutile	.0	.0	.0	.0	.0	.0	.0
Alumina	.0	.0	.0	.0	.0	.0	.0
Calcite	.0	.0	.0	.0	.0	.0	.0
Dolomite	.0	.0	.0	.0	.0	.0	.0
Ankerite	.0	.0	.0	.0	.0	.0	.0
Kaolinite	.0	.0	.0	.2	.2	.0	.3
Montmorillonite	.1	.0	.0	.1	.2	.0	.5
K-Al-Silicate	.1	.0	.0	.2	.1	.3	.7
Fe-Al-Silicate	.0	.1	.0	.0	.0	.0	.1
Ca-Al-Silicate	.0	.1	.0	.0	.0	.0	.2

continued . . .

TABLE 7 (Continued)

EXAMPLE TEST PAGES

	1.0 to 2.2	2.2 to 4.6	4.6 to 10.0	10.0 to 22.0	22.0 to 46.0	46.0 to 100.0	TOTALS
Na-Al-Silicate	.0	.0	.0	.0	.0	.0	.0
Aluminosilicate	.0	.0	.0	.0	.1	.0	.1
Mixed Silicates	.0	.1	.0	.0	.0	.0	.1
Fe-Silicate	.0	.0	.0	.0	.0	.0	.0
Ca-Silicate	.0	.0	.0	.0	.0	.0	.0
Ca-Aluminate	.1	.0	.0	.0	.0	.0	.1
Pyrite	.0	.0	.0	.2	.6	1.1	1.9
Pyrrhotite	.0	.0	.0	.0	.0	.0	.0
Gypsum	.0	.0	.0	.0	.0	.0	.0
Barite	.0	.0	.0	.1	.0	.0	.1
Apatite	.0	.0	.0	.0	.0	.0	.0
Ca-Al-P	3.0	14.5	24.1	2.0	.2	.3	44.1
KCl	.0	.0	.0	.0	.0	.0	.0
Gypsum/Barite	.0	.1	.2	.0	.0	.0	.2
Gypsum/Al-Silic	.0	.0	.0	.0	.0	.0	.0
Si-Rich	.1	.0	.0	.2	.2	.8	1.3
Ca-Rich	.1	.3	.2	.0	.0	.0	.7
Unknown	9.8	18.6	15.3	.8	.3	.0	44.9
Totals	13.8	34.8	40.8	4.8	2.6	3.1	100.0

EXAMPLE TEST PAGE 4

Weight Percent Mineral Basis

	1.0 to 2.2	2.2 to 4.6	4.6 to 10.0	10.0 to 22.0	22.0 to 46.0	46.0 to 100.0	TOTALS
Quartz	.2	.9	1.0	.8	.7	.7	4.4
Iron Oxide	.0	.0	.0	.0	.0	.0	.1
Periclase	.0	.0	.0	.0	.0	.0	.0
Rutile	.0	.0	.0	.0	.0	.0	.0
Alumina	.0	.0	.0	.0	.0	.0	.0
Calcite	.0	.0	.0	.0	.0	.0	.0
Dolomite	.0	.0	.0	.0	.0	.0	.0
Ankerite	.0	.0	.0	.0	.0	.0	.0
Kaolinite	.0	.0	.0	.2	.1	.0	.3
Montmorillonite	.1	.0	.0	.1	.2	.0	.4
K-Al-Silicate	.1	.0	.0	.2	.1	.3	.6

continued . . .

TABLE 7 (Continued)

EXAMPLE TEST PAGES

	1.0 to 2.2	2.2 to 4.6	4.6 to 10.0	10.0 to 22.0	22.0 to 46.0	46.0 to 100.0	TOTALS
Fe-Al-Silicate	.0	.1	.0	.0	.0	.0	.1
Ca-Al-Silicate	.0	.1	.0	.0	.0	.0	.2
Na-Al-Silicate	.0	.0	.0	.0	.0	.0	.0
Aluminosilicate	.0	.0	.0	.0	.0	.0	.1
Mixed Silicates	.0	.1	.0	.0	.0	.0	.1
Fe-Silicate	.0	.0	.0	.0	.0	.0	.0
Ca-Silicate	.0	.0	.0	.0	.0	.0	.0
Ca-Aluminate	.1	.0	.0	.0	.0	.0	.1
Pyrite	.1	.0	.0	.4	1.0	1.9	3.4
Pyrrhotite	.0	.0	.0	.0	.0	.0	.0
Gypsum	.0	.0	.0	.0	.0	.0	.0
Barite	.1	.0	.0	.2	.0	.0	.2
Apatite	.0	.0	.0	.0	.0	.0	.0
Ca-Al-P	3.0	14.6	24.2	2.0	.2	.3	44.3
KCl	.0	.0	.0	.0	.0	.0	.0
Gypsum/Barite	.0	.1	.2	.0	.0	.0	.3
Gypsum/Al-Silic	.0	.0	.0	.0	.0	.0	.0
Si-Rich	.1	.0	.0	.2	.2	.7	1.3
Ca-Rich	.1	.3	.2	.0	.0	.0	.7
Unknown	9.5	18.1	14.8	.8	.3	.0	43.5
Totals	13.6	34.2	40.4	5.0	3.0	3.9	100.0

EXAMPLE TEST PAGE 6

Mineral Area % Coal Basis

	1.0 to 2.2	2.2 to 4.6	4.6 to 10.0	10.0 to 22.0	22.0 to 46.0	46.0 to 100.0	TOTALS
Quartz	.004	.016	.017	.015	.012	.012	.075
Iron Oxide	.000	.000	.000	.000	.000	.000	.001
Periclase	.000	.000	.000	.000	.000	.000	.000
Rutile	.000	.000	.000	.000	.000	.000	.000
Alumina	.000	.000	.000	.000	.000	.000	.000
Calcite	.000	.000	.000	.000	.000	.000	.000
Dolomite	.000	.000	.000	.000	.000	.000	.000
Ankerite	.000	.000	.000	.000	.000	.000	.000
Kaolinite	.000	.000	.000	.003	.002	.000	.006

continued . . .

TABLE 7 (Continued)

EXAMPLE TEST PAGES

	1.0 to 2.2	2.2 to 4.6	4.6 to 10.0	10.0 to 22.0	22.0 to 46.0	46.0 to 100.0	TOTALS
Montmorillonite	.001	.001	.000	.002	.004	.000	.008
K-Al-Silicate	.001	.000	.000	.003	.002	.005	.011
Fe-Al-Silicate	.000	.001	.000	.000	.000	.000	.001
Ca-Al-Silicate	.001	.002	.000	.000	.000	.000	.003
Na-Al-Silicate	.000	.000	.000	.000	.000	.000	.000
Aluminosilicate	.001	.000	.000	.001	.001	.000	.002
Mixed Silicates	.000	.001	.000	.000	.000	.000	.001
Fe-Silicate	.000	.000	.000	.000	.000	.000	.000
Ca-Silicate	.001	.000	.000	.000	.000	.000	.001
Ca-Aluminate	.001	.000	.000	.000	.000	.000	.001
Pyrite	.001	.000	.000	.004	.009	.017	.031
Pyrrhotite	.000	.000	.000	.000	.000	.000	.000
Gypsum	.001	.000	.000	.000	.000	.000	.001
Barite	.001	.000	.000	.002	.000	.000	.002
Apatite	.000	.000	.000	.000	.000	.000	.000
Ca-Al-P	.050	.238	.395	.032	.004	.005	.723
KCl	.000	.000	.000	.000	.000	.000	.000
Gypsum/Barite	.000	.001	.003	.000	.000	.000	.004
Gypsum/Al-Silic	.001	.000	.000	.000	.000	.000	.001
Si-Rich	.001	.000	.000	.004	.004	.013	.022
Ca-Rich	.002	.006	.004	.000	.000	.000	.012
Unknown	.161	.306	.251	.014	.005	.000	.737
Totals	.227	.572	.670	.079	.043	.052	1.642

EXAMPLE TEST PAGE 7

Weight % Coal Basis

	1.0 to 2.2	2.2 to 4.6	4.6 to 10.0	10.0 to 22.0	22.0 to 46.0	46.0 to 100.0	TOTALS
Quartz	.008	.029	.032	.027	.022	.023	.140
Iron Oxide	.001	.000	.000	.001	.000	.000	.002
Periclase	.000	.000	.000	.000	.000	.000	.000
Rutile	.000	.000	.000	.000	.000	.000	.000
Alumina	.000	.000	.000	.000	.000	.000	.000
Calcite	.000	.000	.000	.000	.000	.000	.000
Dolomite	.000	.000	.000	.000	.000	.000	.000

continued . . .

TABLE 7 (Continued)

EXAMPLE TEST PAGES

	1.0 to 2.2	2.2 to 4.6	4.6 to 10.0	10.0 to 22.0	22.0 to 46.0	46.0 to 100.0	TOTALS
Ankerite	.000	.000	.000	.000	.000	.000	.000
Kaolinite	.000	.000	.000	.006	.005	.000	.010
Montmorillonite	.002	.001	.000	.004	.007	.000	.014
K-Al-Silicate	.002	.000	.000	.006	.004	.009	.020
Fe-Al-Silicate	.000	.003	.000	.000	.000	.000	.003
Ca-Al-Silicate	.001	.004	.000	.000	.000	.000	.005
Na-Al-Silicate	.000	.000	.000	.000	.000	.000	.000
Aluminosilicate	.001	.000	.000	.001	.002	.000	.004
Mixed Silicates	.000	.002	.000	.000	.000	.000	.002
Fe-Silicate	.000	.000	.000	.000	.000	.000	.000
Ca-Silicate	.001	.000	.000	.000	.000	.000	.001
Ca-Aluminate	.002	.000	.000	.000	.000	.000	.002
Pyrite	.002	.000	.000	.013	.032	.061	.108
Pyrrhotite	.000	.000	.000	.000	.000	.000	.000
Gypsum	.001	.000	.000	.000	.000	.000	.001
Barite	.002	.000	.000	.006	.000	.000	.008
Apatite	.000	.000	.000	.000	.000	.000	.000
Ca-Al-P	.098	.469	.778	.063	.007	.009	1.424
KCl	.000	.000	.000	.000	.000	.000	.000
Gypsum/Barite	.001	.002	.006	.000	.000	.000	.010
Gypsum/Al-Silic	.001	.000	.000	.000	.000	.000	.001
Si-Rich	.003	.000	.000	.007	.007	.024	.041
Ca-Rich	.004	.010	.007	.000	.000	.000	.021
Unknown	.306	.581	.477	.026	.009	.000	1.399
Totals	.436	1.101	1.299	.160	.095	.125	3.217

EXAMPLE TEST PAGE 8

Distribution By % of Each Mineral Phase

	1.0 to 2.2	2.2 to 4.6	4.6 to 10.0	10.0 to 22.0	22.0 to 46.0	46.0 to 100.0	TOTALS
Quartz	5.4	20.6	22.6	19.4	15.8	16.2	100.0
Iron Oxide	61.2	.0	.0	38.8	.0	.0	100.0
Periclase	.0	.0	.0	.0	.0	.0	.0
Rutile	.0	.0	.0	.0	.0	.0	.0
Alumina	.0	.0	.0	.0	.0	.0	.0

continued . . .

TABLE 7 (Continued)

EXAMPLE TEST PAGES

	1.0 to 2.2	2.2 to 4.6	4.6 to 10.0	10.0 to 22.0	22.0 to 46.0	46.0 to 100.0	TOTALS
Calcite	100.0	.0	.0	.0	.0	.0	100.0
Dolomite	.0	.0	.0	.0	.0	.0	.0
Ankerite	.0	.0	.0	.0	.0	.0	.0
Kaolinite	.0	.0	.0	55.3	44.7	.0	100.0
Montmorillonite	14.6	7.1	.0	26.4	51.9	.0	100.0
K-Al-Silicate	9.8	.0	.0	29.4	18.1	42.8	100.0
Fe-Al-Silicate	.0	100.0	.0	.0	.0	.0	100.0
Ca-Al-Silicate	21.7	78.3	.0	.0	.0	.0	100.0
Na-Al-Silicate	.0	.0	.0	.0	.0	.0	.0
Aluminosilicate	25.7	.0	.0	32.8	41.5	.0	100.0
Mixed Silicates	.0	100.0	.0	.0	.0	.0	100.0
Fe-Silicate	.0	.0	.0	.0	.0	.0	.0
Ca-Silicate	100.0	.0	.0	.0	.0	.0	100.0
Ca-Aluminate	100.0	.0	.0	.0	.0	.0	100.0
Pyrite	2.2	.0	.0	11.8	29.7	56.3	100.0
Pyrrhotite	.0	.0	.0	.0	.0	.0	.0
Gypsum	100.0	.0	.0	.0	.0	.0	100.0
Barite	22.1	.0	.0	77.9	.0	.0	100.0
Apatite	.0	.0	.0	.0	.0	.0	.0
Ca-Al-P	6.9	32.9	54.6	4.5	.5	.6	100.0
KCl	.0	.0	.0	.0	.0	.0	.0
Gypsum/Barite	10.1	24.4	65.4	.0	.0	.0	100.0
Gypsum/Al-Silic	100.0	.0	.0	.0	.0	.0	100.0
Si-Rich	6.3	.0	.0	18.4	17.0	58.3	100.0
Ca-Rich	20.6	48.2	31.2	.0	.0	.0	100.0
Unknown	21.9	41.5	34.1	1.9	.7	.0	100.0
Totals	13.8	34.8	40.8	4.8	2.6	3.1	100.0

continued . . .

TABLE 7 (Continued)

EXAMPLE TEST PAGES

EXAMPLE TEST PAGE 9

Number of Particles in Each Size Range

	1.0 to 2.2	2.2 to 4.6	4.6 to 10.0	10.0 to 22.0	22.0 to 46.0	46.0 to 100.0	TOTALS
Quartz	13.0	12.0	3.0	43.0	7.0	2.0	80.0
Iron Oxide	1.0	.0	.0	1.0	.0	.0	2.0
Periclase	.0	.0	.0	.0	.0	.0	.0
Rutile	.0	.0	.0	.0	.0	.0	.0
Alumina	.0	.0	.0	.0	.0	.0	.0
Calcite	1.0	.0	.0	.0	.0	.0	1.0
Dolomite	.0	.0	.0	.0	.0	.0	.0
Ankerite	.0	.0	.0	.0	.0	.0	.0
Kaolinite	.0	.0	.0	9.0	2.0	.0	11.0
Montmorillonite	3.0	1.0	.0	6.0	2.0	.0	12.0
K-Al-Silicate	2.0	.0	.0	8.0	2.0	1.0	13.0
Fe-Al-Silicate	.0	1.0	.0	.0	.0	.0	1.0
Ca-Al-Silicate	2.0	2.0	.0	.0	.0	.0	4.0
Na-Al-Silicate	.0	.0	.0	.0	.0	.0	.0
Aluminosilicate	1.0	.0	.0	2.0	1.0	.0	4.0
Mixed Silicates	.0	1.0	.0	.0	.0	.0	1.0
Fe-Silicate	.0	.0	.0	.0	.0	.0	.0
Ca-Silicate	2.0	.0	.0	.0	.0	.0	2.0
Ca-Aluminate	3.0	.0	.0	.0	.0	.0	3.0
Pyrite	3.0	.0	.0	9.0	6.0	3.0	21.0
Pyrrhotite	.0	.0	.0	.0	.0	.0	.0
Gypsum	2.0	.0	.0	.0	.0	.0	2.0
Barite	2.0	.0	.0	5.0	.0	.0	7.0
Apatite	.0	.0	.0	.0	.0	.0	.0
Ca-Al-P	146.0	192.0	77.0	78.0	4.0	1.0	498.0
KCl	.0	.0	.0	.0	.0	.0	.0
Gypsum/Barite	2.0	1.0	1.0	.0	.0	.0	4.0
Gypsum/Al-Silic	2.0	.0	.0	.0	.0	.0	2.0
Si-Rich	4.0	.0	.0	7.0	2.0	2.0	15.0
Ca-Rich	7.0	5.0	1.0	.0	.0	.0	13.0
Unknown	492.0	270.0	50.0	40.0	4.0	.0	856.0
Totals	688.0	485.0	132.0	208.0	30.0	9.0	1552.0

TABLE 7 (Continued)

EXAMPLE TEST PAGES

EXAMPLE TEST PAGE 10

Distribution of Mineral Phases - Frequency Percent

Total Number of Points	=	1552.0
% Quartz	=	5.2
% Iron Oxide	=	.1
% Periclase	=	.0
% Rutile	=	.0
% Alumina	=	.0
% Calcite	=	.1
% Dolomite	=	.0
% Ankerite	=	.0
% Kaolinite	=	.7
% Montmorillonite	=	.8
% K-Al-Silicate	=	.8
% Fe-Al-Silicate	=	.1
% Ca-Al-Silicate	=	.3
% Na-Al-Silicate	=	.0
% Aluminosilicate	=	.3
% Mixed Silicates	=	.1
% Fe-Silicate	=	.0
% Ca-Silicate	=	.1
% Ca-Aluminate	=	.2
% Pyrite	=	1.4
% Pyrrhotite	=	.0
% Gypsum	=	.1
% Barite	=	.5
% Apatite	=	.0
% Ca-Al-P	=	32.1
% KCl	=	.0
% Gypsum/Barite	=	.3
% Gypsum/Al-Silicate	=	.1
% Si-Rich	=	1.0
% Ca-Rich	=	.8
% Unknown	=	55.2

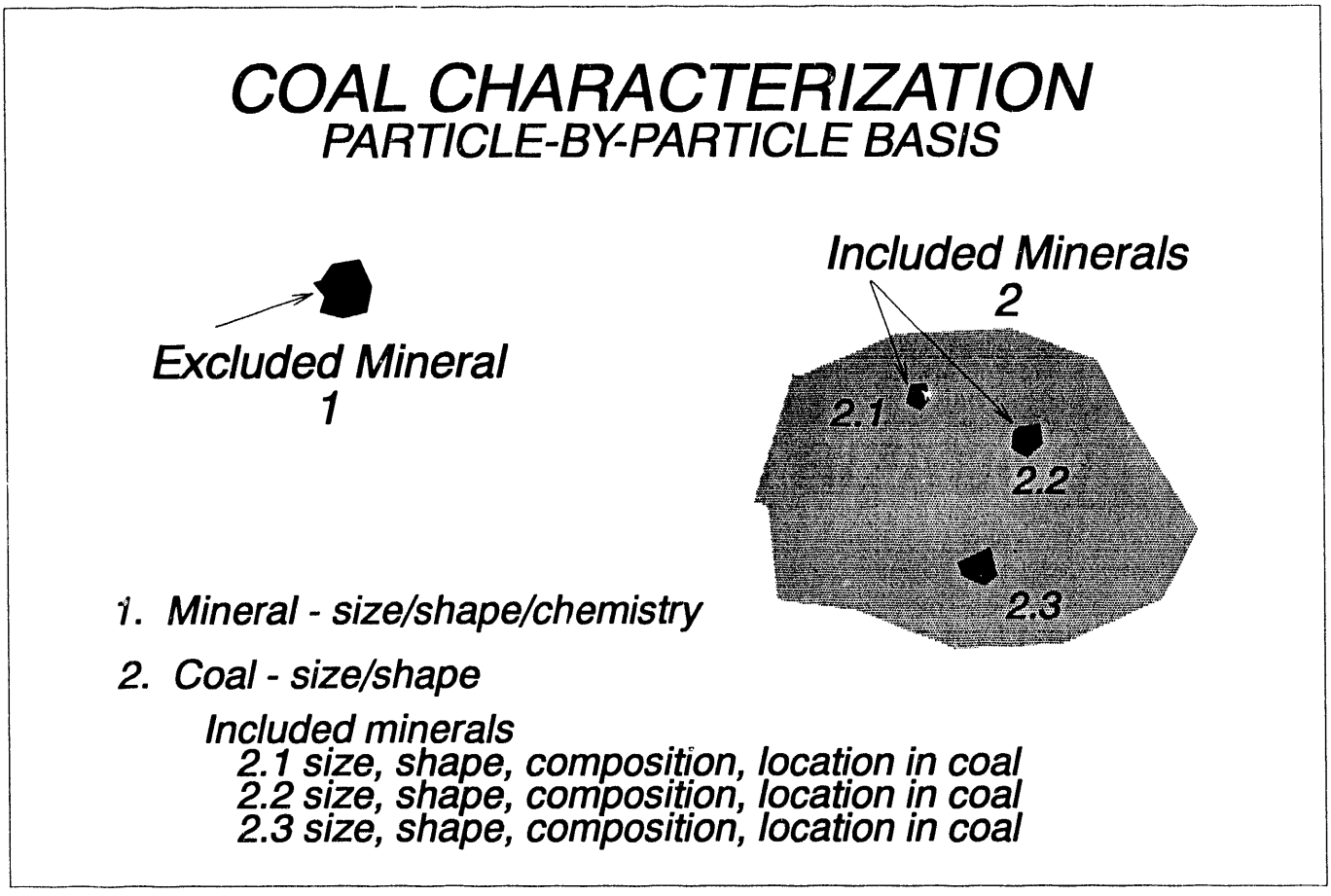

Figure 11. Characterization of coal particles and minerals on a particle-by-particle basis.

2.4 Conclusions

Mineral standards and coal samples were prepared for testing of the CCSEM routine. The chemical typing routine in the CCSEM program correlated well with the standard minerals. Some errors in the routine appear to be in the quantification of the minerals by the Tracor Northern PRC (Particle Recognition and Characterization) program. Problems may be due to the dwell time used as well as the magnifications and step sizes used. The reproducibility tests showed poor precision in obtaining a mineral definition of the sample, but showed better reproducibility in the bulk particle-size distributions obtained. New procedures and software are presently being developed to address these problems. Preliminary investigations into a round-robin testing of the present CCSEM method have been made.

Automation of the CCSEM analysis, which allows the analysis to be run unattended, was completed. Interfacing between CCSEM and image analysis has also been completed. This allows the fields analyzed by the CCSEM routine to be stored in the image analysis system and data concerning the juxtaposition to be collected.

More graphic outputs for the CCSEM program have been developed, and work continues in this area. An improved version of the data manipulation program has been developed and is now being tested.

Future programs will include some of the graphic methods as standard outputs. Further development of coal minerals analysis may well focus on the sole use of the sophisticated imaging capabilities now available. Ultimately, the present chemical typing and sizing may be replaced by chemical typing and characterization on the new system. The method proposed to accomplish this was outlined above in the section entitled "Planned Developments." I feel an intermediate step which would combine the present analysis with modern imaging capabilities is prudent for achieving the sound data needed. The present chemical typing and characterization has the benefit of thousands of hours of use and testing. By combining it with the new imaging capabilities, we can solve one problem at a time and move forward in a logical, stepwise fashion. For these reasons, we will further explore the capabilities of the image analysis system, while continuing to test and explore the capabilities of the present system.

3.0 TASK 2: MINERAL AND ASH CHARACTERIZATION

3.1 Introduction

The important thrust of this task is to determine the inorganic constituents of coal, char, and fly ash using CCSEM, SEMPC, AES, and x-ray photoelectron spectroscopy (XPS). Samples will be generated from drop-tube furnace reactors at both the EERC and PSIT. Also included in this task is a separate 3-year study of inorganic transformations observed for the Robinson and Eagle Butte coals combusted in a down-fired combustor.

3.2 Equipment and Procedures

CCSEM utilizes a computer program to locate, size, and analyze particles. Because the analysis is automated, a large number of particles can be analyzed quickly and consistently. The main component of the CCSEM analysis system is the annular backscattered electron imaging (BEI) detector. The BEI system is used because the coefficient of backscatter (the fraction of the incoming beam that is backscattered) is proportional to the square root of the atomic number of the scattering atoms. This permits a high degree of resolution between sample components based on their atomic numbers. This means that minerals can be easily discerned from the coal or char matrix, and fly ash particles can be easily discerned from epoxy in polished sections. Brightness and contrast controls are used to optimize threshold levels between the coal or char matrix and mineral grains or fly ash particles. When a video signal falls between these threshold values, a particle is discerned, and the particle center is located. A set of eight diameters about the center of the particle is measured, and the particle area, perimeter, and shape are calculated. The beam is then repositioned to the center of the particle, and an x-ray spectrum is obtained. The information is then stored for data reduction and manipulation. The CCSEM data provides quantitative information concerning the discrete mineral species or noncrystalline inorganic phases present and their

size and shape characteristics. Since the same analysis can be performed on the initial coal, char, and resultant fly ash, direct comparisons can be made and inorganic transformations inferred.

In addition to the CCSEM analysis of coal to determine size and type of minerals, the technique has recently been expanded to determine the juxtaposition of minerals; i.e., how minerals are associated with each other and whether mineral grains are associated within coal particles (inherent) or associated extraneously to coal particles. This information is extremely important with respect to understanding the transformations of inorganic constituents during combustion. In order to perform such an analysis, image analysis is employed that allows for detailed examination and manipulation of stored secondary and backscattered electron images and x-ray maps. Included and excluded minerals and associations of adjacent minerals are determined easily by examining stored images of coal-epoxy polished surfaces. This technique is currently under development at EERC, and results have been published elsewhere (8).

Characterization of fly ash was performed using scanning electron microscopy and electron microscopy analysis. A technique was developed at EERC to determine the relative abundance of phases present in ashes and deposits (9). The technique is called SEM point count or SEMPC. The method involves microprobe analysis of about 250 random points in a polished cross section of sample. The quantitative analysis of each point is transferred to a computer file for data base analysis. New Fortran software is used to calculate molar and weight ratios for each point. Using these ratios, the points that have compositions of known phases (common to ashes and coal minerals) are identified and counted. The software then finds the relative number of unknown phases. The unknown phases are those for which there are no known phases corresponding to the chemical composition. For this study, it was assumed that these points were amorphous. In addition, the average chemical composition of all the points in the sample was calculated.

X-ray photoelectron spectroscopy (XPS) and Auger spectroscopy were used to characterize the surface of the fly ash and char. The XPS technique determines the binding energy of an electron removed from the outer 50 angstroms of the surface due to the impingement of beam x-rays. The binding energy of the electrons is a function of the elements present on the surface and their chemical compositions. The Auger technique uses the electron beam as the ionization source, and the Auger electrons that come from the secondary electron emission are measured. This technique can provide chemical composition data for very small areas on the order of one square micrometer. Thus the Auger technique can be used to examine the first 20 to 50-angstrom depths of surface layers of individual fly ash particles.

Another surface analysis technique performed at the EERC is secondary ion mass spectroscopy (SIMS). SIMS is a surface analysis and depth profiling technique that utilizes an ion beam to bombard the sample. This produces emissions of positive and negative secondary ions from the surface. These ions, both individual and clusters of atoms, are mass-analyzed with an energy-filtered quadruple mass spectrometer. The technique is used for trace impurity analysis and offers extremely high detection sensitivity for many elements, full elemental detection (include hydrogen), and the ability to provide isotopic and molecular information.

3.3 Analysis of PSIT Deposits and Ash

As part of collaborative efforts between EERC and PSIT, fourteen deposits generated by PSIT were analyzed using SEMPC. The deposits, listed in Table 8, were generated from the following coals: San Miguel, Beulah, Kentucky #11, Illinois #6, Kentucky #9, Eagle Butte, and Upper Freeport. Table 9 summarizes the mineral phase and elemental oxide compositions for the deposits. Four fly ash samples were analyzed as well as using CCSEM analysis. These ashes were generated by PSIT from the following coals: Kentucky #9, Eagle Butte, San Miguel, and Illinois #6.

3.4 Characterization of Inorganics in Ash Using Surface Science Techniques

Several coal chars and ashes generated in the EERC drop-tube furnace were analyzed by surface science techniques to determine particle surface chemistry and coating structure. The major techniques used during this reporting period were AES and AES depth profiling utilizing an ion sputtergun. The char particles analyzed were typically 30-60 μm in diameter.

Eagle Butte chars produced in the drop-tube furnace at residence times of 0.5 and 0.8 seconds were analyzed. A typical char particle from the 0.5 second sample had abundant, very small ash particles on the surface (Figure 12a). Calcium was a major constituent of the ash and occurred in lesser amounts in the char. Figure 12b is a calcium distribution map of Figure 12a and shows areas of low calcium where there are fewer ash particles. The occurrence of calcium in the char appears to be limited to the outer portion of the char particle. A depth profile taken on the char surface shows a decline in the amount of calcium present toward the interior (Figure 12c). The zone of calcium enrichment was about 40 angstroms in thickness.

A char particle from the 0.8 second Eagle Butte sample showed a calcium-rich coating masking the underlying structure (Figure 13a). The structure was readily apparent after sputtering away the surface of the particle (Figure 13b). The coating seems to be comprised of many very small ash particles. A hollow sphere or bubble appears at the lower left corner of the char particle. This is either an attached cenosphere coated with fine ash or a bubble formed by outgassing behind the coalescing fine ash. A depth profile of the particle surface revealed the coating to be composed of calcium oxide and about 30 angstroms thick (Figure 13c).

Eagle Butte fly ash particles can show inhomogeneities in the near surface zones. Sputtering of the surface produces differential etching of more resistant particles imbedded in the surface (Figure 14a,b,c). Also revealed are surface layers which are probably coatings of fine ash. A depth profile shows that the surface layer of calcium oxide is about 75 angstroms thick and covers an ash particle that is richer in sulfur (Figure 14d).

Beulah char generated in the drop-tube furnace at a residence time of 0.1 second was analyzed. A typical char particle was covered with calcium-rich ash (Figure 15a). Some of the ash coalesced into larger masses, especially along the lower portion of the particle. AES analysis of the

TABLE 8

PSI DEPOSIT SAMPLE LABELS AND EERC SAMPLE NUMBERS

Sample Label	
San Miguel SM-3	Kentucky #11 KY-2
San Miguel SM-5	Kentucky #11 KY-5
San Miguel SM-6	Illinois #6 IL-4
San Miguel SM-11	Illinois #6 IL-5
Beulah Lignite BL-19	Kentucky #9 KY-16
Beulah Lignite BL-21	Eagle Butte EB-17
Beulah Lignite BL-29	Upper Freeport UF-13

TABLE 9

SEMPC ANALYSIS OF PSIT DEPOSITS
(EDS WEIGHT PERCENTS)

Phase Composition	SM-3	SM-5	SM-6	SM-11	BL-19	BL-21	BL-29	KY-2	KY-5	IL-4	IL-5	KY-16	EB-17	UF-13
Gehlenite	0.0	0.0	0.8	0.0	3.7	15.8	6.0	0.0	1.8	0.0	0.0	0.0	5.5	0.0
Anorthite	1.2	0.6	0.8	1.1	1.9	0.0	0.0	10.3	5.5	1.8	1.7	0.0	3.6	0.0
Pyroxene	0.0	0.0	0.0	0.0	0.0	1.8	0.0	0.0	0.0	0.0	0.0	0.0	1.8	1.8
Mullite	0.0	0.0	0.0	0.0	0.0	0.0	0.0	0.0	0.0	0.0	10.3	0.0	1.8	0.0
Calcium Silicate	0.0	0.0	0.0	0.0	0.0	0.0	2.0	0.0	0.0	0.0	0.0	0.0	0.0	0.0
Quartz	7.8	6.3	47.7	8.9	33.3	0.0	14.0	15.5	29.1	5.5	8.6	26.2	12.7	35.7
Iron Oxide	0.6	0.0	1.2	0.7	18.5	3.5	2.0	19.0	7.3	5.5	8.6	7.1	3.6	7.1
Calcium Oxide	0.0	0.0	0.8	0.0	0.0	1.8	0.0	0.0	0.0	0.0	0.0	0.0	0.0	0.0
Ankerite (Ca,Mg,Fe)	0.0	0.0	0.4	0.0	0.0	0.0	0.0	0.0	0.0	0.0	0.0	0.0	0.0	0.0
Aluminum Oxide	0.0	0.0	0.0	0.0	0.0	0.0	0.0	0.0	0.0	0.0	1.7	0.0	0.0	0.0
Pure Kaolinite Amorp.	0.6	2.5	0.4	0.7	0.0	0.0	0.0	0.0	0.0	0.0	15.5	0.0	1.8	1.8
Kaolinite Derived	0.0	1.3	0.4	0.0	0.0	3.5	0.0	0.0	7.3	25.5	1.7	2.4	5.5	0.0
Illite (Amorp.)	26.9	19.6	9.5	15.1	0.0	5.3	2.0	3.4	5.5	9.1	8.6	7.1	1.8	7.1
Montmorillonite Amorp.	0.0	0.0	0.0	0.0	0.0	0.0	0.0	0.0	0.0	0.0	0.0	14.3	0.0	0.0
Calcium-Derived	0.0	0.0	0.4	0.0	0.0	0.0	0.0	0.0	0.0	0.0	0.0	0.0	0.0	0.0
Unclassified	62.9	69.6	37.4	73.4	42.6	68.4	74.0	51.7	43.6	52.7	43.1	42.9	61.8	46.4
Oxide Composition														
SiO_2	70.6	70.0	82.6	72.1	51.6	37.5	37.3	49.4	63.4	55.5	44.1	56.6	45.8	65.4
Al_2O_3	17.3	17.8	7.5	15.8	7.8	18.5	7.6	13.7	12.9	20.8	31.7	13.3	17.3	14.2
Fe_2O_3	2.3	1.2	3.0	1.6	23.4	5.2	8.9	24.6	10.9	11.9	16.3	15.0	9.9	12.6
TiO_2	0.9	1.2	0.7	1.2	0.5	0.9	2.1	0.5	1.1	1.0	0.4	1.1	1.0	0.5
P_2O_5	0.0	0.0	0.0	0.0	0.0	0.0	0.0	0.0	0.1	0.0	0.0	0.1	0.2	0.0
CaO	3.6	4.1	3.0	3.9	10.8	21.9	33.8	6.5	6.4	4.7	3.5	6.2	18.6	1.8
MgO	0.5	0.6	0.3	0.5	2.3	6.2	1.3	1.3	0.8	1.5	0.6	0.7	4.1	0.8
Na_2O	1.5	1.7	0.5	1.5	0.9	5.0	0.2	1.0	0.5	0.8	0.6	0.2	0.4	0.4
K_2O	2.7	2.5	1.0	2.2	0.8	2.9	3.6	1.7	2.1	3.0	2.0	3.2	1.3	2.2
SO_3	0.1	0.2	0.3	0.2	0.3	0.6	2.9	0.3	0.2	0.1	0.2	2.1	0.7	0.3
BaO	0.2	0.1	0.1	0.2	0.6	0.9	0.7	0.1	0.1	0.1	0.0	0.1	0.2	0.1
MN_2O_7	0.1	0.2	0.1	0.2	0.4	0.2	0.1	0.2	0.3	0.1	0.1	0.1	0.2	0.4
ClO	0.2	0.3	0.8	0.6	0.6	0.1	1.5	0.8	1.2	0.5	0.5	1.2	0.2	1.3

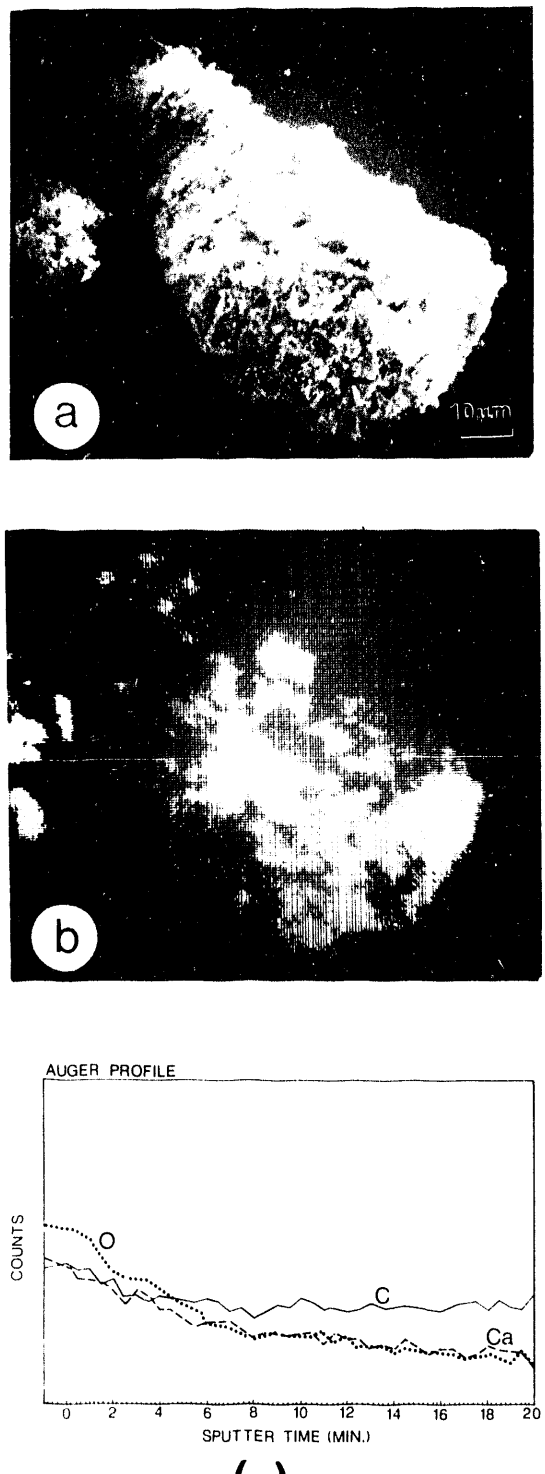

Figure 12. Eagle Butte char, 0.5-second residence time. (a) Char particle covered with ash. (b) Ca distribution map. (c) AES depth profile.

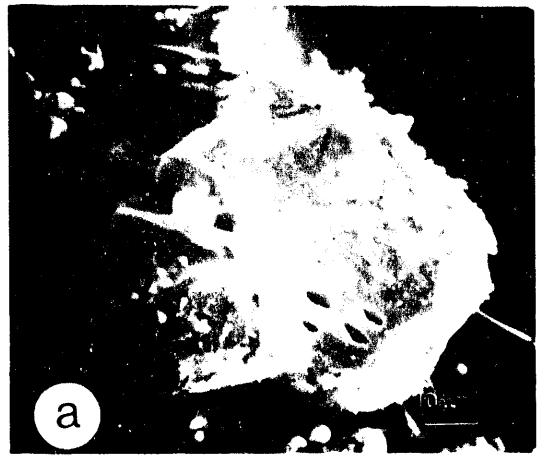

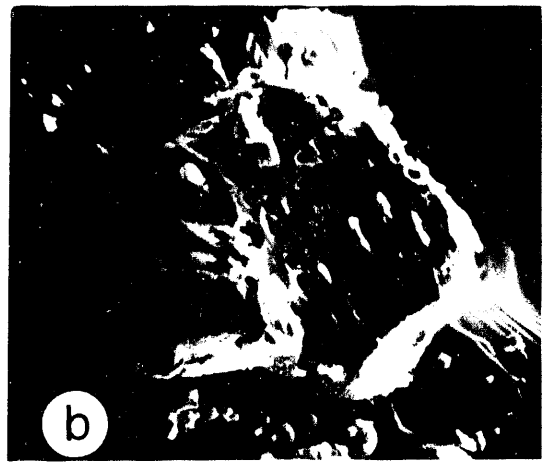

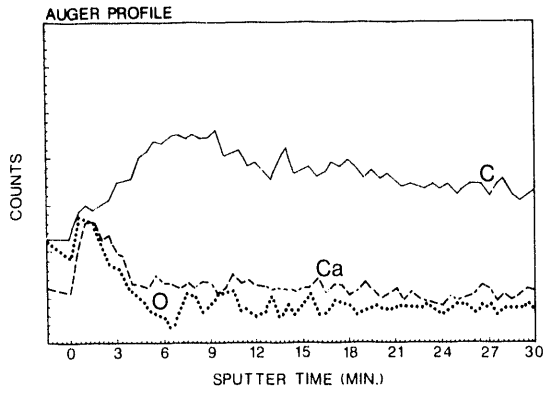

(c)

Figure 13. Eagle Butte char, 0.8-second residence time. (a) Char particle showing calcium oxide coating masking underlying structure. (b) Surface after 30 minute sputter. (c) AES depth profile.

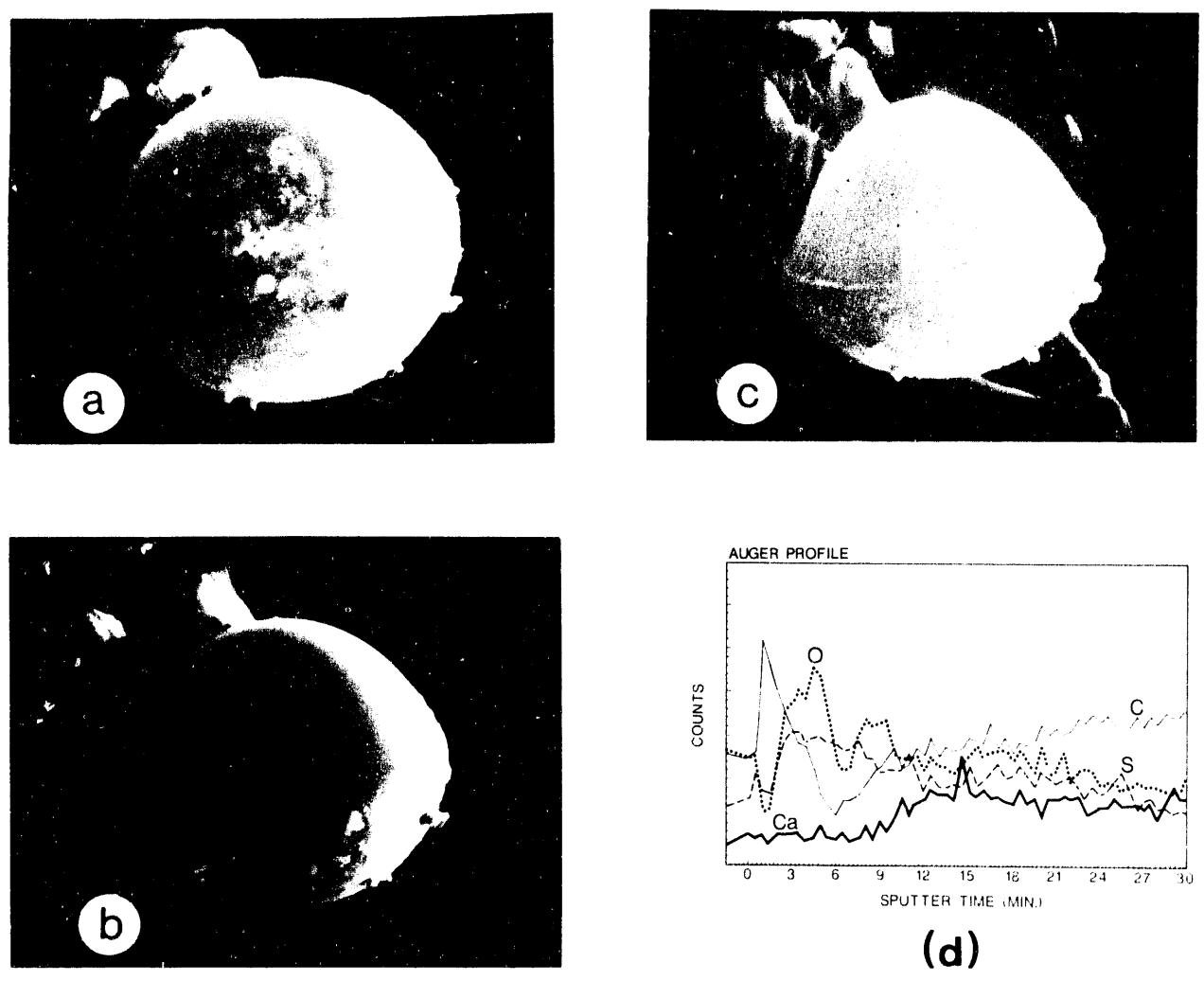

Figure 14. Eagle Butte fly ash, 0.8-second residence time. (a) Ash particle with smaller ash particles adhering to and imbedded in the surface. (b) Surface after 30-minute sputter. (c) Surface after 60-minute sputter. (d) AES depth profile.

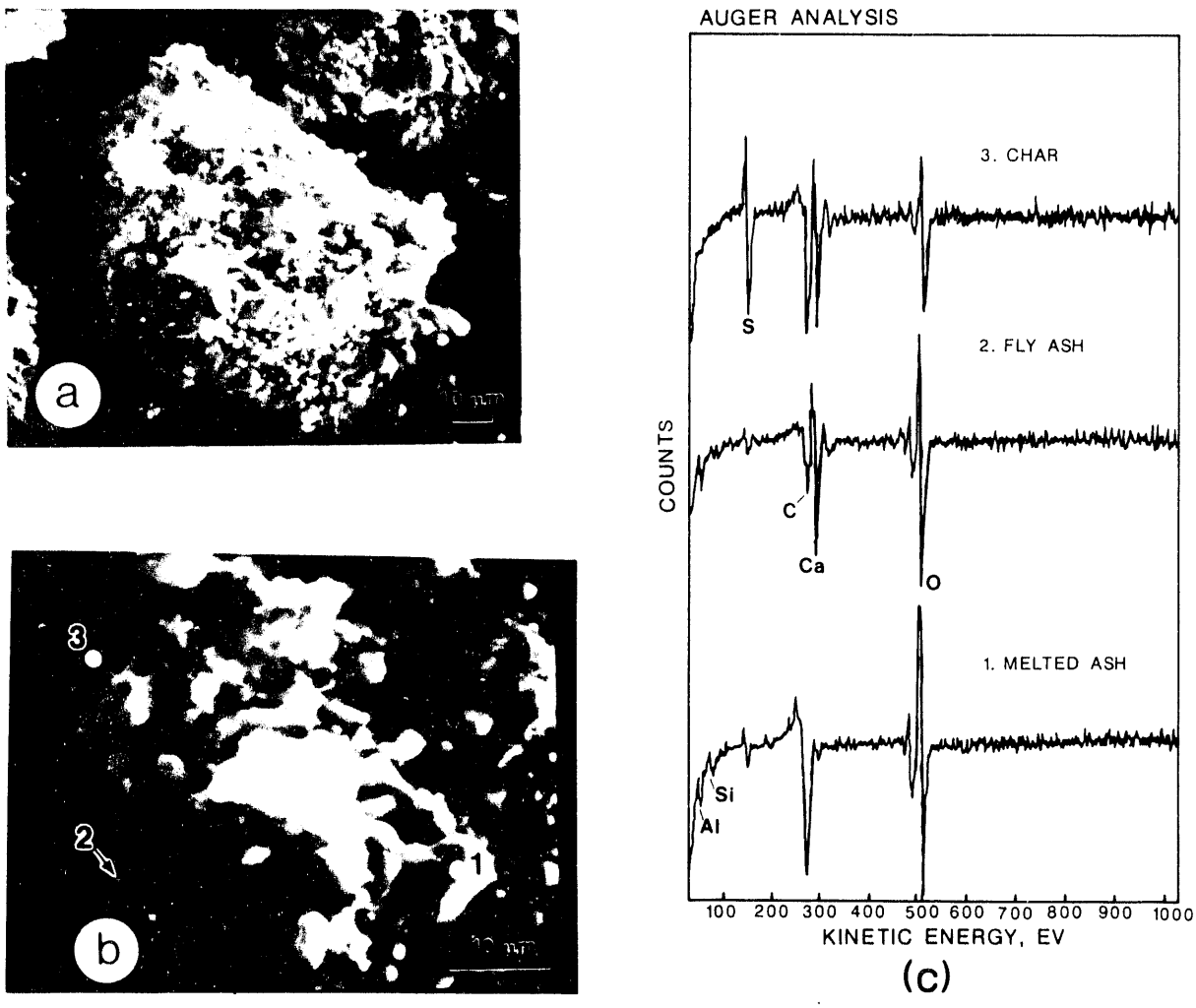

Figure 15. Beulah char, 0.1-second residence time. (a) Char particle covered with ash and coalescing ash. (b) Detailed view of coalescing ash showing AES analysis points. (c) AES point analyses.

various components (Figure 15b,c) revealed the fly ash and melted material to have significantly less sulfur than the char. The small fly ash particle was composed largely of calcium oxide. However, the melted material contained much less calcium than either the ash or char. This is expected if calcium is reacting further and forming other compounds.

An agglomeration of fly ash from the Beulah sample is shown in Figure 16a. Several larger ash particles, including a cenosphere, apparently had stuck together with melted material. Part of the agglomerate was covered with a boxwork-like deposit coating several particles. AES analysis of selected points showed that the melted material and the coating contained significant amounts of sodium, while the fly ash particles had a very minor amount (Figure 16c). All areas analyzed contained iron and sulfur. After sputter-etching the surface in several stages, distinct surface layering became apparent (Figure 17a,b,c). A thin outer layer about 0.3 μm thick was underlain by a layer about 3.5 μm thick, all overlying the core of the particle. AES analysis of the layering revealed the outer layer was higher in silicon than subsequent layers and almost devoid of iron. The core of the particle had similar amounts of iron like the layer immediately above, but almost no sulfur. The cenosphere exposed during sputter-etching appeared to be composed of material similar to the intermediate layer.

Robinson char produced in the drop-tube furnace at a residence time of 0.2 seconds was analyzed. A typical char particle with a mix of fly ash sizes is shown in Figure 18a. AES analysis of a micron-size ash particle revealed the composition to be primarily calcium oxide with no sulfur present (Figure 18b and c). The nearby char contained appreciably less calcium and substantially more sulfur (Figure 18b and c).

Synthetic coal particles were analyzed with AES. The original material consisted of 10% SiO_2, 5% Na, and 1% S in a carbon matrix. Quartz was used for the SiO_2 component, sodium benzoate for the Na component, and pure sulfur powder for the S component. The particles were combusted at 1100°C for 1.5 seconds in a laminar flow furnace, and the fly ash was collected on filter paper.

A typical fly ash particle shown in Figure 19a was 37 μm in diameter and covered with much smaller ash particles less than 1 μm in size (Figure 19a). Analysis of the surface shows the composition to be mainly SiO_2 (Figure 20). This was to be expected knowing the original composition. Elemental Si, possibly from condensation of vaporized Si, was present in significant amounts along with a small amount of sodium. Carbon and sulfur were not present at the surface of the particle. Analysis of a small particle attached to the fly ash showed a composition of SiO_2 and lesser amounts of sodium, sulfur, and carbon (Figure 20).

The large particle in Figure 19a was subjected to sputter-etching with an argon ion gun for 90 minutes. The interior of the particle was heterogeneous as shown by the topography of the sputtered surface. The core of the particle contained small blebs of more resistant material (Figure 19b). Also indicated was a thin outer rind on the fly ash particle. Gas bubbles were present in the interior of the particle. Analysis of the core revealed

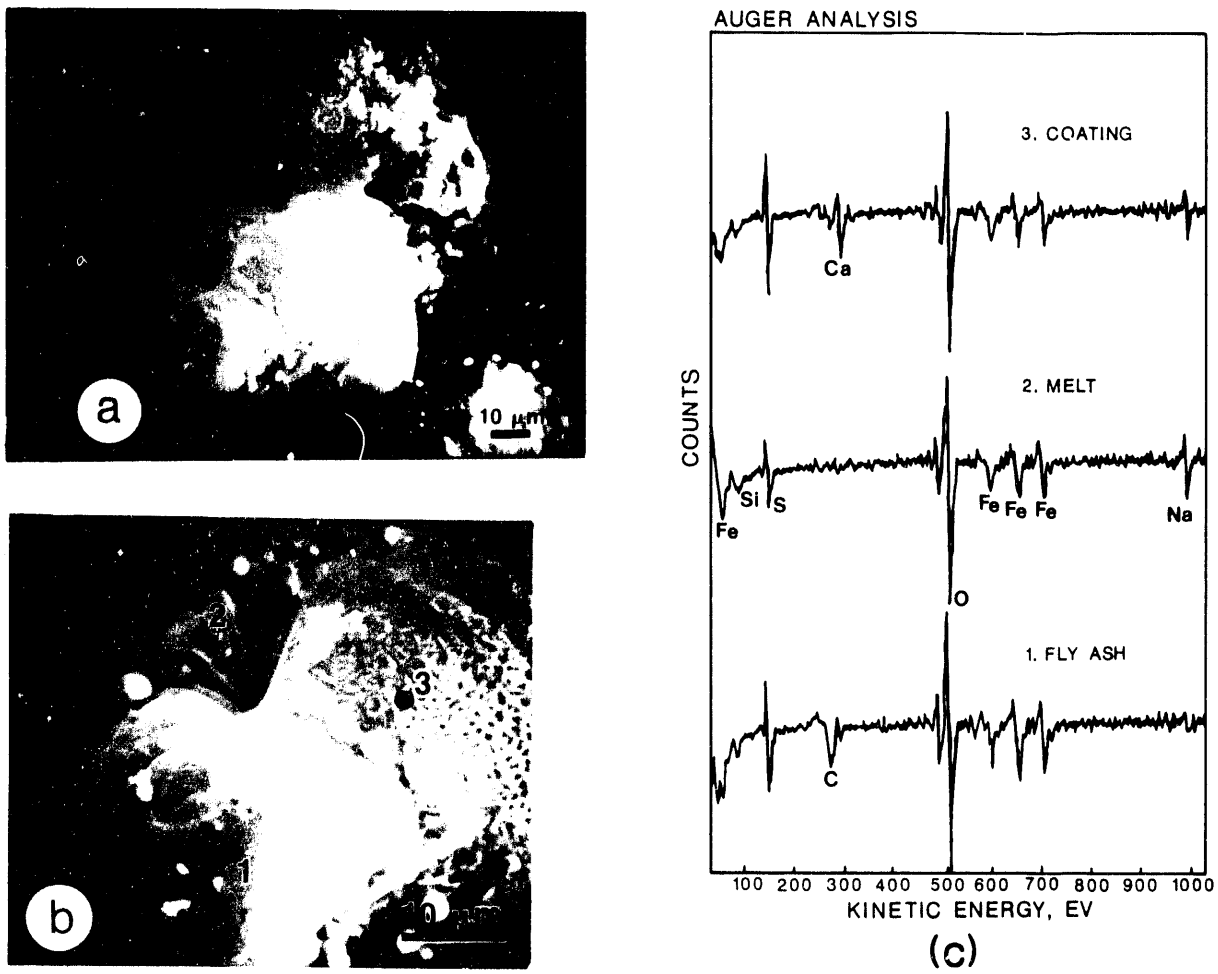

Figure 16. Beulah fly ash agglomerate, 0.1-second residence time. (a) Several fly ash particles sticking together with melted material. (b) Detailed view showing AES analysis points. (c) AES point analyses.

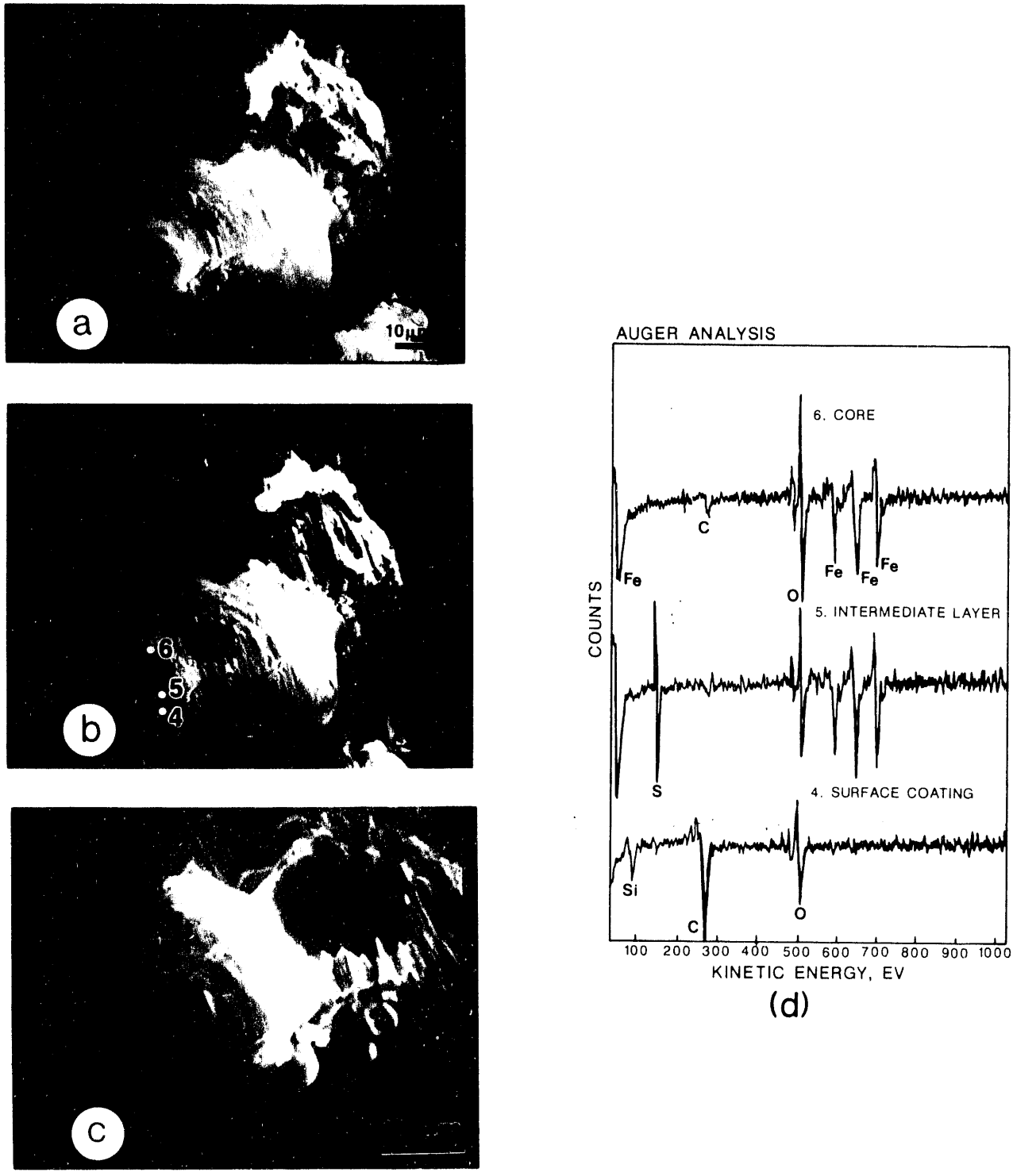

Figure 17. Beulah fly ash agglomerate after ablation of surface layers by ion sputtergun. (a) Surface after 60-minute sputter. (b) Surface after 120-minute sputter showing AES analysis points. (c) Detailed view of sputter agglomerate. (d) AES point analyses.

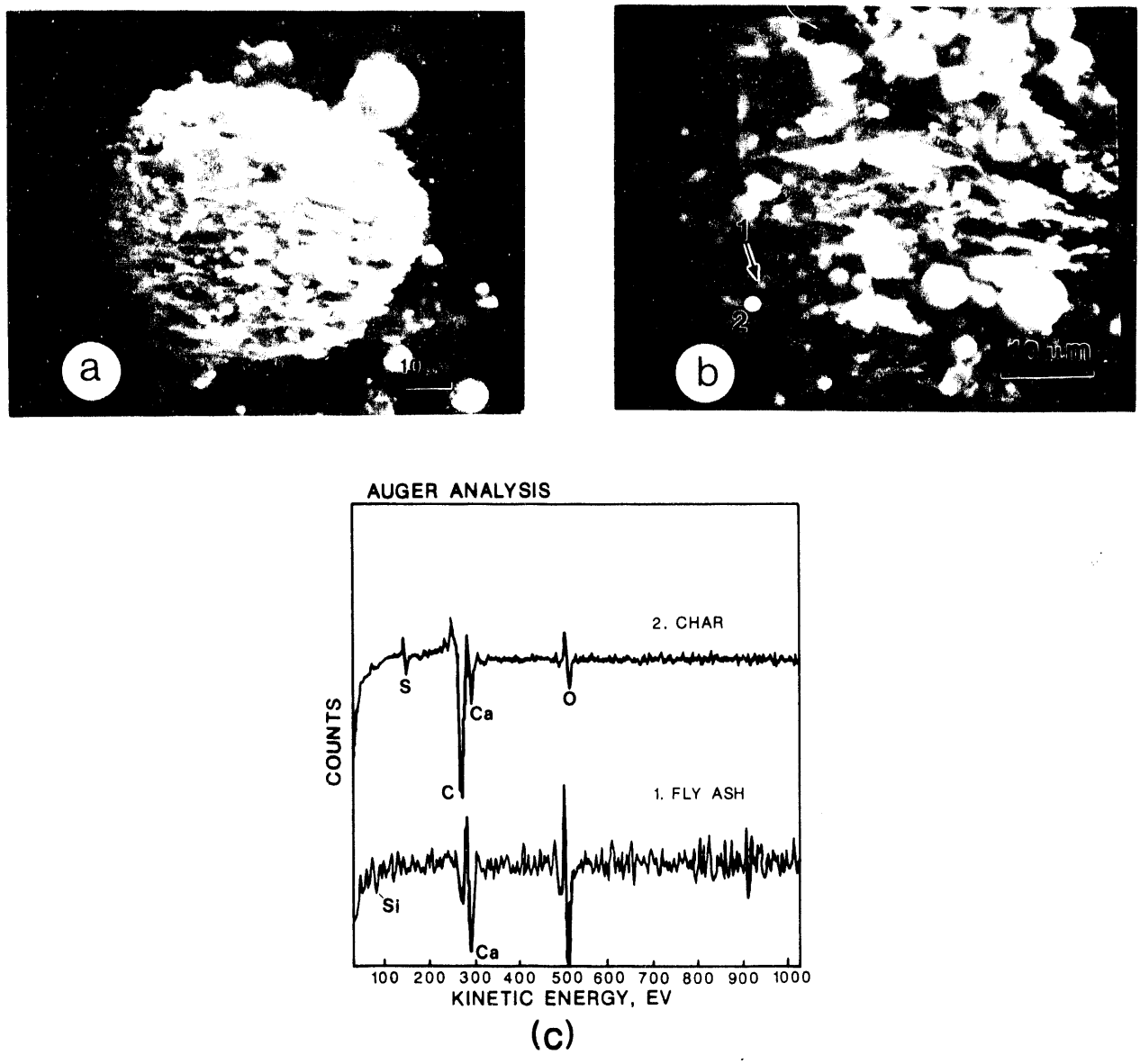

Figure 18. Robinson char, 0.2-second residence time. (a) Char particle covered with multiple sizes of fly ash. (b) Detailed view of char showing AES analysis points. (c) AES point analyses.

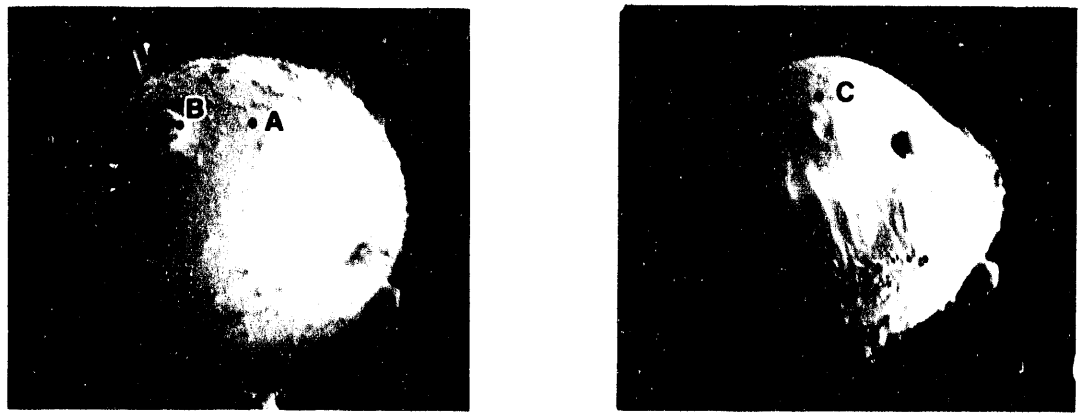

Figure 19. Secondary electron image of a) typical synthetic coal fly ash grain, and (b) fly ash grain after 90-minute argon ion gun sputter.

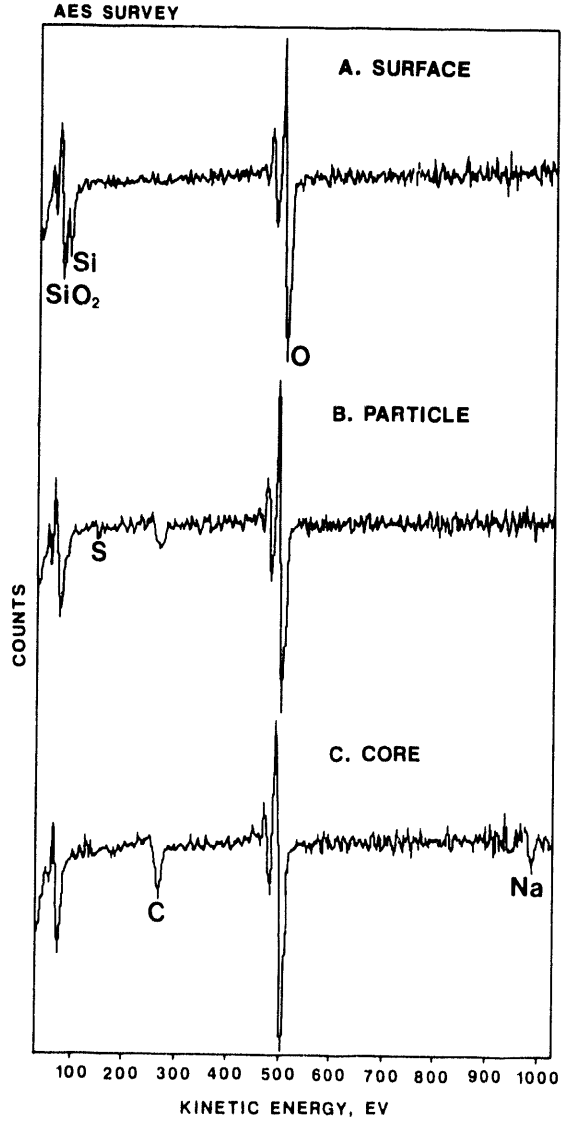

Figure 20. Results of AES generated at two spots on the synthetic fly ash grain surface (a and b) and one spot (c) in the interior of the fly ash grain.

primarily SiO_2 and significant amounts of carbon and sodium. Neither elemental silicon nor sulfur were present (Figure 20). The presence of carbon and sodium suggests the core may contain remnants of the original material, although sulfur is absent. The outer rind is devoid of carbon and sulfur and also contains appreciable silicon.

3.4.1 Conclusions

Several coal chars and ashes generated in the EERC drop-tube furnace were analyzed by surface science techniques to determine particle surface chemistry and coating structure. The major techniques used during this reporting period were Auger electron spectroscopy (AES) and AES depth profiling utilizing an ion sputtergun. The char particles analyzed were typically 30-60 μm in diameter.

Small 0.1-2 μm ash particles observed on the surface of the Eagle Butte char were analyzed using AES. Calcium was a major constituent in the ash particles. Char particles nearing 90% carbon burnout show an enrichment of Ca at the outer 0.3-0.4 μm of their surface using AES depth profiling. Inhomogeneities, in the form of differential etching by the AES sputtergun, are consistently observed in the near surface zone of Eagle Butte fly ash particles. Beulah char shows the same Ca-rich coating as the Eagle Butte char. Chemical depth profiling of Beulah fly ash grains shows distinct variations in chemistry and physical resistance to the sputtering action of the Auger beam.

AES analysis of early-stage, small inorganic ash droplets in the Beulah and Robinson chars also shows very high Ca content.

Synthetic coal ash particles were analyzed with AES. The original material consisted of 10% SiO_2, 5% Na, and 1% S in a carbon matrix. Fly ash was produced in the drop-tube furnace using a combustion temperature of 1100°C and a residence time of 1.5 seconds. Surface analysis revealed large particles, 30-40 μm in diameter, coated with smaller particles less than 1 μm in size. The surface of the large particles was typically SiO_2 with some elemental Si present, possibly vaporized Si condensate, virtually no carbon or sulfur. Small particles attached to larger fly ash grains were observed that were composed of SiO_2 and lesser amounts of sodium, sulfur, and carbon. The interior of the large grains revealed vesicular heterogeneous material of varying resistances to the argon ion sputtergun. Composition of interior material was primarily SiO_2, with significant amounts of carbon and sodium.

3.5 Inorganic Transformations of Low-Rank Coal Studied in a Down-Fired Combustion System

3.5.1 Introduction

This work was conducted by John P. Hurley at The Pennsylvania State University and was part of his Ph.D. thesis. The work was supported by the Combustion Inorganic Transformations (CIT) Project and represents a compilation of three years of work.

3.5.2 The Down-Fired Combustor System

To properly understand the process of ash formation during pulverized low-rank coal combustion, a knowledge of the time-temperature history and interactions of ash particles is required. In addition, representative samples of ash must be collected from the boiler at several stages of the combustion process for laboratory study. Unfortunately, the high degree of swirl and recirculation in boiler, pulverized coal flames makes measuring histories or collecting representative samples in utility boilers difficult. Therefore, as part of an effort to study the formation of ash during pulverized coal combustion, as well as other combustion phenomena, a down-fired combustor of sectional construction was built. The combustor system is designed for self-sustained combustion of pulverized coal in a nonrecirculating and nonswirling flame and to provide easy access for sampling at all stages of combustion.

The down-fired combustor is illustrated in Figure 21. It is substantially different from an earlier combustor built at Pennsylvania State by Howard (10), in that it is larger and does not use water-cooled tubes at the top of the combustor to stabilize the flame in the main combustion chamber. The present combustor is more similar to a combustor built later at Pennsylvania State by Kinneman (11), who performed much of the preliminary design work for the present combustor.

3.5.3 The Preheat System

Before firing pulverized coal, the combustor is preheated on natural gas at an energy input rate of 250,000 Btu/hr. The natural gas burner is inserted into one of the 3-inch ports located directly below the quarl. Preheating continues until the wall temperature profile approximates that of the wall temperature profile encountered when firing the coal to be tested. This usually takes about three hours.

After heating the combustor to a suitable temperature, the natural gas burner is shut down, and firing with pulverized coal begins. The feed rate is usually adjusted so that the energy input to the combustor is approximately 200,000 Btu/hr, which yields a volumetric heat release rate of about 20,000 Btu/hr/ft^3. The feeder is kept on a weighing scale to allow manual monitoring of the feed rate. Once set, the rate has been found to vary by no more than 5% during a run.

3.5.4 Sampling Equipment and Procedures

3.5.4.1 Particulate Sampling Equipment

Gas and particulate sampling can commence as soon as a stable temperature distribution occurs above the sampling point. The particulate sampling probe is illustrated in Figure 22. It is designed to collect particulate matter at an isokinetic rate and at a constant volumetric flow rate when sampling in different regions of the combustor.

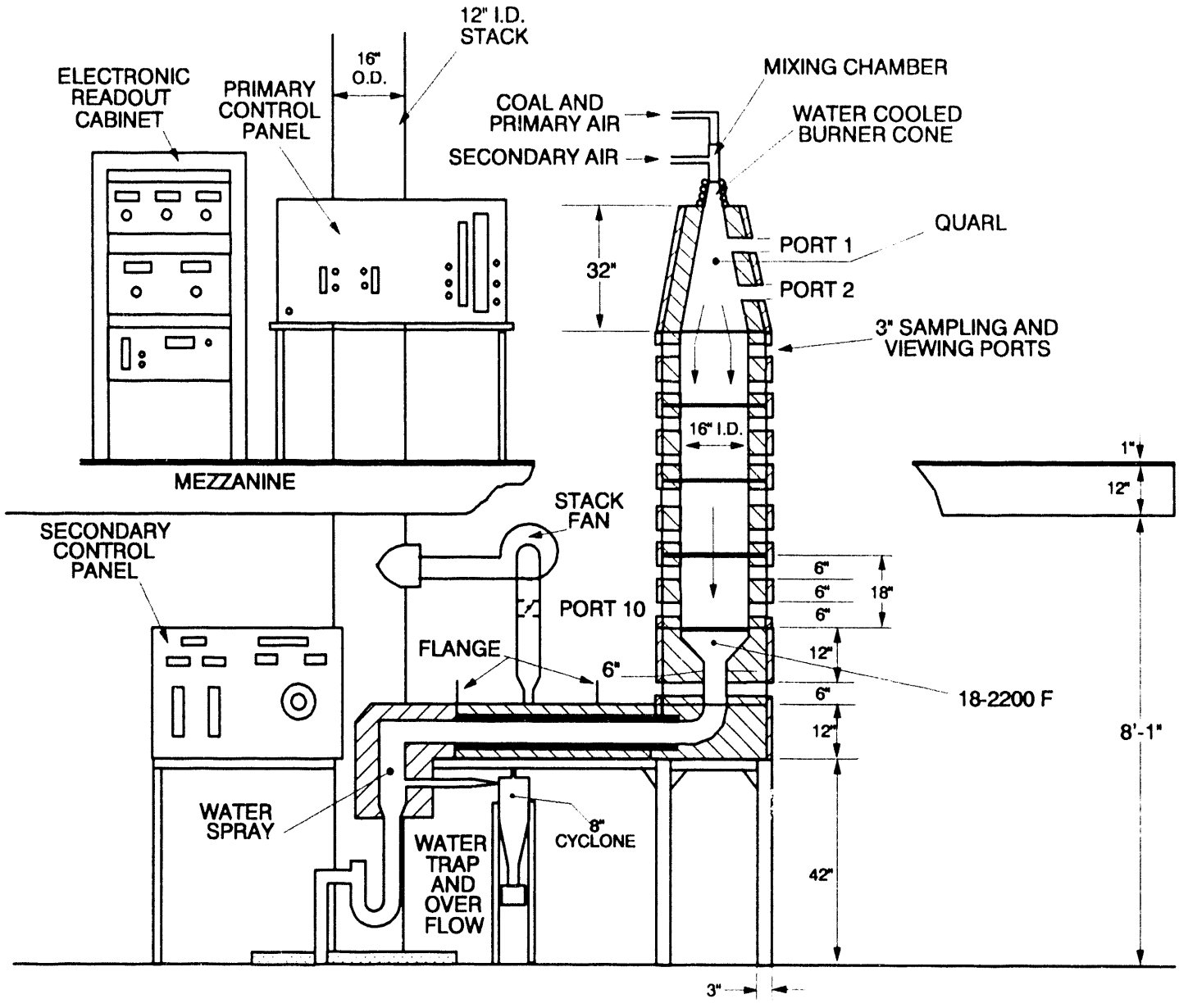

Figure 21. The down-fired combustor.

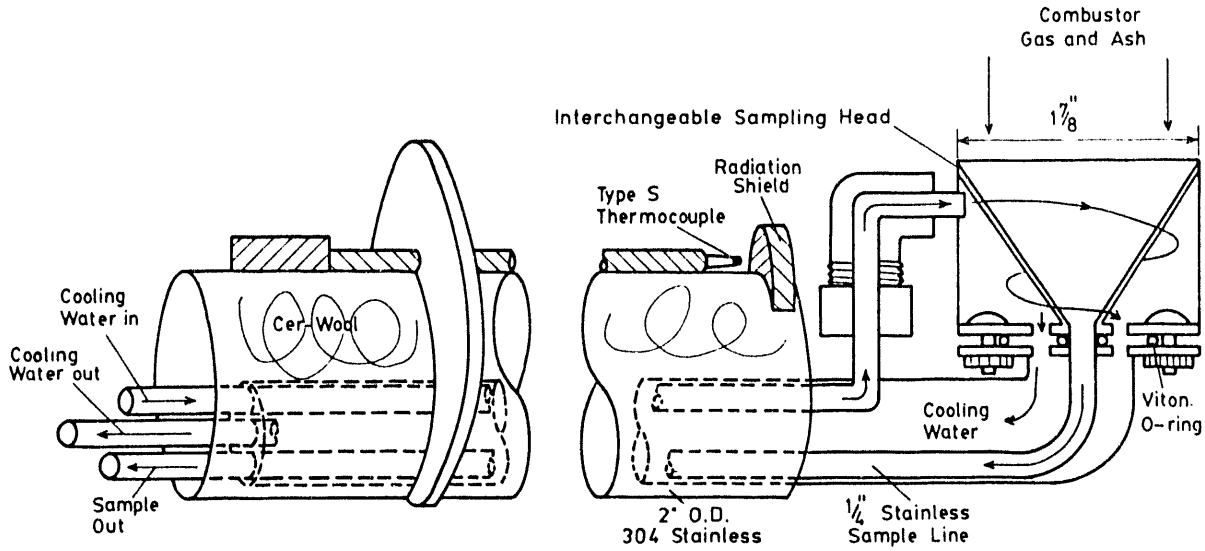

Figure 22. The particulate matter sampling probe.

To make isokinetic sampling possible when the volumetric flow rate is held constant, the sampling probe was designed so that the sampling head is interchangeable with other heads of similar design, but with sampling cones of different diameters. This allows us to pull a constant fraction (1/72) of the total gas flow at an isokinetic rate whether sampling in the main furnace body where the diameter is 16 inches, or at the top of the quarl where the diameter is 8 inches. The diameter of the sampling cone in the head used for sampling in the main combustion chamber is 1 7/8 inches; for the head used at the bottom port of the quarl, the diameter is 1 1/2 inches. The diameter of the cone in the sampling head used at the top of the quarl is 15/16 inches.

The reason that sampling is performed at constant volumetric flow rates (measured at constant temperature) is because the gas and particulate sample are passed through a multicyclone system to separate the particulate matter from the gas. By maintaining a constant flow rate at the cyclones, the 50% cutpoints of each cyclone remain constant.

The multicyclone system used to separate the particulate matter from the gas during particulate collection is a four-stage assembly manufactured by Anderson Samplers Inc. It consists of Cyclones 280-10, 280-2, and 280-5, followed by 65-mm diameter Filter Holder 274. Under normal sampling conditions, the aerodynamic 50% cutpoints are 15 μm for the 280-10, 3.2 μm for the 280-2, and 0.7 μm for the 280-5. The final filter is a polypropylene fiber filter manufactured by Micron Separation Incorporated. It is 99.9% efficient at collecting 0.3 μm and larger particles from an air stream. Although the filter has not been tested on smaller particles, its collection efficiency is expected to be above 95% for 0.1 μm and larger particles.

The dew point for the flue gas produced during combustion of western U.S. low-rank coals in the down-fired combustor is approximately 55°C. To prevent condensation of the flue gas in the sampling system, the outlet temperature of the coolant water to the sampling probe is maintained above 80°C. Also, the sample line between the probe and the multicyclone system is insulated. Finally, the multicyclone system is housed in a convection oven during sampling. The temperature in the oven is maintained at between 90° and 100°C.

The sample gas is pulled through the sample probe and multicyclone system with a Gast model 0822 rotary vane pump. The sample gas is vented to the stack after it has passed through the pump.

The volumetric flow rate through the probe-multicyclone system is monitored with a rotameter situated outside of the oven, between the multicyclone system and the pump. The flow rate is controlled with a 1/2-inch gate valve on the inlet side of the flow meter. Pressure drop across the sample probe and multicyclone is measured with a vacuum gauge placed between the gate valve and the multicyclone. The pressure measured at that point gives a good indication of the degree of filter loading so that preparations can be made to end the sampling run before the filter becomes blocked. Pressure in the flowmeter is measured at the outlet of the flowmeter with another vacuum gauge. The reading of that gauge is used to correct the measured flow to 0 psig.

3.5.4.2 Temperature Measurement

Gas temperatures in the combustor are measured with a suction pyrometer. Gas temperatures were also measured with a bare Type S thermocouple. Although the bare thermocouple bead is not as accurate as the suction pyrometer in measuring gas temperatures, it is much easier to use. Therefore, once a relationship between the gas temperature measured by the suction pyrometer and the temperature measured by the bare thermocouple was established, the bare thermocouple was used, and the temperature it indicated was corrected to the actual gas temperature.

3.5.4.3 Gas Sampling

Gas samples are collected using a water-cooled stainless steel probe. The water coolant flow is regulated so that the temperature of the gas exiting the probe is over 80°C. As the gas exits the probe, it passes through a high-capacity filter to remove particulate matter. It then flows into a heated teflon sample line held at 100°C. The temperature of the gas is kept above the dew point to prevent condensation of water, which could possibly dissolve SO_2.

Gas composition is monitored continuously with a bank of on-line gas analyzers kept in an instrument cabinet near the combustor. The gas flow is split into two streams at the cabinet. One stream passes through a refrigeration unit to remove moisture from the gas, and then on to O_2, CO_2, and CO meters situated in parallel to each other. The O_2 meter is a Beckman model 755 that uses a paramagnetic detection system. The CO and CO_2 detectors are Beckman model 864 infrared detectors.

The other gas stream is diverted to a Thermo Electron Corporation model 900 gas conditioner unit that dilutes the gas so that the dew point of the gas is below the operating temperatures of the SO_2 and NO_x meters that follow. The SO_2 meter is a Thermo Electron Corporation model 40 that uses a pulsed fluorescent detector. The NO_x meter is a Thermo Electron Corporation model 10 that uses a chemiluminescent detector.

Gas flow through the detectors is provided by two diaphragm pumps situated in the detector cabinet. After passing through the detectors, the gas is exhausted to the stack.

3.6 Analytical Equipment and Procedures

A variety of analyses were performed on the coals and combustor samples produced in this study. The standard analyses were proximate, ultimate, sulfur, Btu, x-ray diffraction (XRD), chemical fractionation, and inorganic elemental analyses. More in-depth analyses of the samples included computer-controlled scanning electron microscopy (CCSEM) in conjunction with energy-dispersive x-ray spectrometry (EDS), transmission electron microscopy (TEM), and scanning transmission electron microscopy (STEM) in conjunction with EDS.

3.6.1 Standard Analyses

Proximate analyses were performed using two methods. The bulk coals were analyzed with a Leco Corporation MAC-400 proximate analyzer. Because of the limited sample supply available, proximate analysis of the combustor samples were performed with a thermogravimetric analyzer (TGA). The TGA procedure required only 10 milligrams of sample, whereas MAC-400 analysis required at least 500 milligrams. Two different TGAs were used: a Perkin Elmer 7 Series Thermal Analysis System, and a DuPont 951 TGA module in conjunction with a DuPont 1090 Thermal Analyzer, which was used for data acquisition and manipulation. The heating and gas flow programs used with each instrument were the same except for initial purge times and were designed to approximate the heating and gas flow parameters used in the ASTM coal proximate analysis.

Ultimate analyses were also performed on samples of each coal. The ultimate analyses were performed with a Leco Corporation CHN-600. Sulfur analyses were performed on each coal and cyclone sample with a Leco Corporation SC-132 sulfur determinator. Heating values of the coals were determined with a Parr adiabatic calorimeter. Inorganic elemental analysis of each coal and cyclone sample was performed by lithium metaborate fusion, followed by dissolution in 4% HNO_3, and analysis of the solution with a Spectrometrics Spectrospan 3 direct current plasma spectrometer (DCP). The inorganic elements analyzed for by the DCP are Na, Mg, Al, Si, K, Ca, Ti, Mn, Fe, Sr, and Ba. X-ray diffraction analysis of each sample was performed with a Phillips XRG 3100 x-ray diffractometer employing Cu Kα radiation. Peak identifications were made with the assistance of the Phillips SANDMAN software.